



Structural and Mechanical Properties of Directionally Solidified Al-Si Alloys

S.P. Nikanorov, V.N. Osipov, and L.I. Regel

(Submitted April 19, 2018; in revised form September 20, 2019; published online December 2, 2019)

This review covers research aimed at finding the optimum composition and growth rate to obtain a highly modified Al-Si alloy using directional solidification. Investigations of microstructure and mechanical properties as a function of Si content and growth rate are analyzed. These works show that the composition yielding a eutectic microstructure changes considerably with increasing solidification rate in the range of 10^2 – 10^4 $\mu\text{m/s}$. The increase in ultimate tensile strength with increasing Si content up to that giving a completely eutectic microstructure is explained by a redistribution of volume content of α -Al and eutectic. The increase in tensile strength with increasing rate is explained by a decrease in microstructural scale accompanying the transformation of flake-to-fiber eutectic microstructure. The optimal fine fiber structure without any primary crystals of Al-Si alloy at a given Si content is obtained at the solidification rate giving a completely eutectic microstructure at that composition. Hypereutectic alloys can be fully modified using rapid cooling at such solidification rate that causes coupled growth of the eutectic for given composition of the alloy. Additional Sr modification results in a super-modified structure, high tensile strength and record high elongation.

Keywords Al-Si alloy, directional solidification, elongation, eutectic point, microstructure, tensile strength

1. Introduction

The binary Al-Si system is the basis of aluminum-silicon casting alloys in which silicon is the major alloying element. These alloys are called “silumins.” The manufacture of these alloys constitutes over 90% of all aluminum-based castings. Al-Si alloys are used as construction materials for different purposes, as well as solder for aluminum like Al-Ge. Heat-resistant aluminum alloys are used for car engine parts such as connecting rods, rocker arms, cylinders, pistons and valve retainers (Ref 1, 2). Construction alloys usually have a hypoeutectic content of silicon. Alloys for other applications are eutectic or hypereutectic in Si. This is connected primarily to ductility decreasing with increasing Si content. Other elements are added to these alloys to increase the strength and improve some other properties. The search continues for optimal additions and optimal Si content for different applications of cast alloys based on the Al-Si system. This search will be aided by analysis of published information on the dependence of structural and mechanical properties on Si content, solidification rate and modification of Al-Si alloy.

The effects of Si content in hypoeutectic alloys and low rates of solidification have been well studied. There are also many results for very high rates of solidification, 10^5 – 10^6 $\mu\text{m/s}$. Presented here are the results of such investigations obtained

predominantly during the last decade for alloys of near eutectic and hypereutectic compositions at rates up to 10^4 $\mu\text{m/s}$. Such rates are the most interesting for applications. The regions of Si content under consideration are determined by conventional casting processes: For slow cooling rate processes (sand, plaster, investment), the range is 5–7 wt.%, for permanent molds 7–9 wt.%, and for die castings 8–12 wt.% Si. Hypereutectic Al-Si alloys of 13 wt.% and higher Si content are obtained by die casting and thixo-forging technologies. That is why in this review investigation of 7–15 wt.% Si alloys are mainly described. Conclusions on improving technology based on the results of these investigations focus on hypereutectic alloys.

Here, results of directional solidification of alloys are analyzed because in this case there is opportunity to control the thermodynamic parameters of solidification.

2. Structure of Binary Alloys

2.1 Component Concentration Effect

Physical and mechanical properties of alloys are determined by microstructure, which depends on composition and conditions of solidification and cooling such as rate, temperature gradient and convection. According to the equilibrium phase diagrams, at low freezing rates coupled solidification of Al-Si and Al-Ge components takes place at eutectic compositions equal to 12.6 wt.% Si (Ref 3) and 52 wt.% Ge (Ref 4). This coupled solidification results in a fine microstructure consisting of the two phases, sometimes as alternating lamellae and sometimes as fibers of one phase in the other. At fast solidification rates, coupled solidification moves toward increasing Si or Ge content. Earlier, this displaced point had been called the quasi-eutectic point because the microstructure is like that which is formed at low freezing rates from the eutectic composition. Following current practice, here we call

S.P. Nikanorov and V.N. Osipov, Ioffe Institute, Politekhnikeskaya Str. 26, Saint Petersburg 194021, Russia; and L.I. Regel, Clarkson University, Potsdam, NY 13699-5700. Contact e-mail: s.nikanorov@mail.ioffe.ru.

this the eutectic microstructure, even though it may not have formed at the equilibrium eutectic composition.

The most informative data on the dependence of the microstructure of Al-Si alloys on Si content and the rate of solidification were presented in Ref 5. In Ref 6, the range of investigated Si concentrations was expanded. Figure 1 shows a diagram of microstructure of Al-Si alloys versus composition and solidification rate as determined experimentally in Ref 5, with some changes and additions based on other works. In Ref 5, the microstructure is divided into modified (fiber) and unmodified (flake), apparently due to the morphology of the primary silicon phase. Dotted line 3 divides hypo- and hypereutectic alloys with flake eutectic plus primary α -Al crystals of dendritic structure and flake eutectic plus Si primary crystals structure. This line is attached to the 12.6 wt.% Si eutectic point. The upper border between flake Si and fiber regions was extended up to 35 wt.% Si in Ref 6.

The points along line 4 of the diagram show the Si concentration of samples in Ref 6. These samples were prepared by casting molten Al-Si alloy in a levitated state into a massive Cu mold under a He atmosphere. According to a rough estimate, the solidification rate V was about $5 \times 10^3 \mu\text{m/s}$. The Al-11.5 wt.% Si alloy consisted of eutectic and dendrites of primary α -Al crystals. A fine eutectic structure with star-like crystals of silicon was observed in alloys with 25 wt.% Si. The concentration and size of Si crystals increased with increasing Si content. Star-like primary Si crystals corresponded to 30 wt.% and massive crystals to 35 wt.% Si. The authors (Ref 6) considered that the Al-20 wt.% Si alloy has a nearly eutectic structure at about $5 \times 10^3 \mu\text{m/s}$ solidification rate.

The points along line 5 in Fig. 1 show the composition of alloys investigated in Ref 7. The alloys were obtained by directional solidification using Stepanov's method (Ref 8).

Rods were pulled up from the melt through a special air-cooling shaper at a rate of $10^3 \mu\text{m/s}$. According to Ref 8, the temperature gradient in the cooling zone while pulling rods from a melt in Ref 7 was about 10 K/mm.

Metallographic sections of the samples are shown in Fig. 2. In samples with 8, 10, 11.7 and 13 wt.% Si α -Al dendrites and eutectic matrix were observed. The volume fraction of the α -Al dendrite phase decreased with increasing Si content. The dendrites of primary α -Al crystals were mainly oriented in the direction of pulling the sample from the melt. The eutectic matrix is the phase consisting of α -Al and silicon fibers, which are commonly referred to as eutectic silicon. The eutectic fibers in Al-8 wt.% Si alloy were about 1-1.5 μm in length and 0.3 μm in thickness. The Al-15 wt.% Si alloy had a eutectic structure. Primary α -Al dendrite crystals were absent. The vermiform silicon crystals of the eutectic had a mean length of about 1-1.5 μm . The alloys with 20 and 25 wt.% Si consisted of the eutectic matrix and primary silicon crystals of dendrite and star-like structure. At a solidification rate of $10^2 \mu\text{m/s}$, a eutectic structure without α -Al dendrites was observed for a Si content of about 11.7 wt.%. In general, the results in Ref 6, 7 for the dependence of microstructure on the silicon content correspond to the diagram in Ref 5. There was a small difference in the structure of eutectic silicon at a solidification rate of about $10^3 \mu\text{m/s}$ for alloys with Si content from 8 to 11.7 wt.% (line 5). According to Ref 7, samples with a Si content up to 11.7 wt.% had a eutectic flake structure and dendritic primary α -Al crystals. However, in Ref 5, a fibrous eutectic structure with α -Al dendrites was observed in that range of Si content. They preferred to speak about a "modified" rather than a fiber structure and noted that the velocity for transition of the structure on line 1 of the diagram is accurate to only $\pm 50\%$.

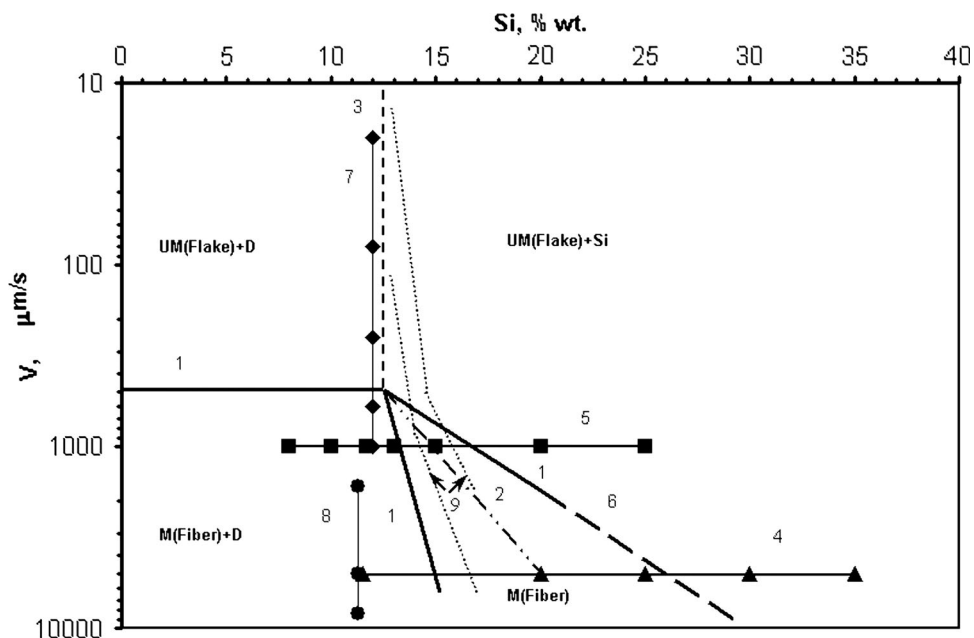


Fig. 1 Diagram of Al-Si alloys microstructure. Lines 1 are the boundaries between the regions of different microstructure according to Ref 5. In particular, the higher line 1 divides the region of flake eutectic plus α -Al dendrite structure, D , from that for fiber eutectic plus D . Dashed line 3 divides the regions of flake eutectic plus α -Al dendrite structure, D , from that for flake eutectic plus primary Si crystals structure for solidification rates lower than $480 \mu\text{m/s}$. Dashed line 6 extrapolates the upper border of the fiber region to a solidification rate of about $10^4 \mu\text{m/s}$. The lines 4, 5, 7 and 8 correspond to Si content and the solidification rate of alloys investigated in Ref 6, 7, 86, 47, respectively. The dotted lines 9 are borders of the zone of coupled solidification of eutectic (Ref 9). Stroke-dotted line 2 connects points corresponding to conditions of obtaining fine fibrous microstructure without primary crystals (Ref 7) or with rare separate Si crystals (Ref 6)

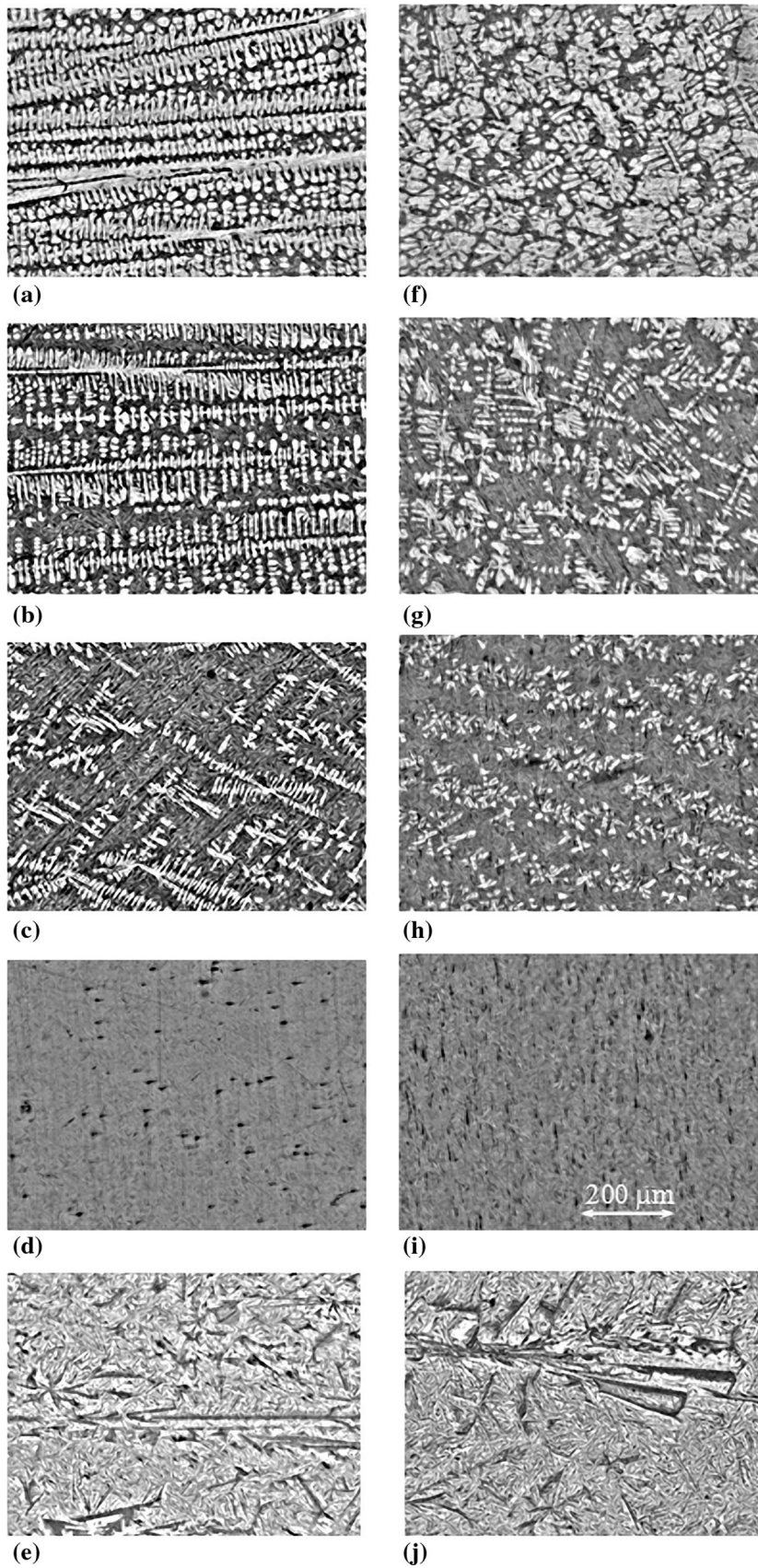


Fig. 2 Microstructure of Al-Si alloys containing Si: 8 (a, f); 11.7 (b, g); 13 (c, h); 15 (d, i); 20 (e), and 25 (j) wt.% Si; (a-e) and j is a longitudinal section; (f-i) are cross sections (Ref 7)

Experimental data in Ref 6, 7 give the possibility to select line 2, which corresponds to the conditions for formation of the fiber eutectic structure without primary α -Al or Si crystals, or with their solitary dendrites. The dependence of the microstructure of Al-Si alloys with 12-17 wt.% Si on solidification rate was studied from 10 to $10^3 \mu\text{m/s}$ in Ref 9. A narrow zone of coupled growth of eutectic without primary crystals of either Al or Si was found in that work. Line 2 is close to the upper bound of a zone of coupled growth (Ref 9). It is necessary to note that no zone of coupled growth was observed at a growth rate lower than $480 \mu\text{m/s}$ in the work (Ref 5) as opposed to Ref 9. We think that this difference can be connected with superheating the melt before casting in Ref 9.

In Ref 10, the morphology of the silicon phase in Al-Si alloys was presented on a diagram of Si content versus solidification rate. Borders between different structures in Ref 10 are slightly different from those in Ref 5. Particularly, at low rates of solidification, the existence of angular, rod and complex regular structures of primary Si was found, in addition to the flake (unmodified) silicon structure. This difference may be due to different methods of measuring the rate of solidification. It is important that the line for the flake-fiber transition in Ref 10 corresponds to line 2 of Fig. 1 as revealed in Ref 7.

Here, it is worth noting that, recently, similar intensive research was performed on the effect of thermal gradient, solidification rate and alloying with refractory and rare earth metals on structure and strength properties of eutectic alloys based on Ni-Al (Ref 11, 12).

2.2 Solidification Rate Effect

2.2.1 Macrostructure. It is well known that the mechanical properties of alloys depend on both macrostructure (shape, size and distribution of grains) and microstructure (structure within grains). Columnar grains in a conventional casting nucleate and grow from the mold surface. There is a higher temperature gradient near the wall of the mold than in the volume. Solidification of the melt in the form of a columnar structure is in the opposite direction from the heat flow. Closer to the center of the ingot, the temperature gradient decreases and the growth of equiaxed grains occurs. The growth of equiaxed grains leads to increasing isotropy of the ingot's structure and its mechanical properties. The type of grain structure is important for applications of the material.

With controlled directional solidification, the macrostructure is homogeneous and does not change with position. Such a situation takes place with solidification by the Bridgman method and by Stepanov's technique. The structure can be changed by an alteration of the thermal conditions and the freezing rate, thereby modifying the mechanical properties. Therefore, macrostructural investigations are considered here briefly.

Investigations of the columnar-to-equiaxed transition in hypoeutectic Al-Si alloys were performed by upward unidirectional solidification experiments under unsteady-state conditions (Ref 13, 14). Such conditions enabled simulation of solidification at typical industrial foundry processes. The experimental setup consisted of a water-cooled mold with heat extracted from the bottom, promoting vertical upward directional solidification. Radial heat losses were minimized by special thermal insulation. The bottom part of the mold was

closed with a thin carbon steel sheet, which physically separated the metal from the cooling fluid. The thermal behavior during solidification was monitored via fine thermocouples positioned along the length of the mold. Experiments were carried out under conditions designed to avoid natural convection due to density variations either from temperature differences (cooling from the bottom) or from the solute-enriched liquid, which is denser than the melt itself. Details were given in Ref 15-17. It was found (Ref 14) that the columnar-equiaxed transition in Al-Si alloys of 3, 5, 7 and 9 wt.% Si was sharp. The character of the transition did not depend on Si content. No influence of the solute content on the macrostructure transition in Al-Si alloys was also observed in Ref 18. The cooling rate at the transition was close to the critical value of about 0.17 K/s at a growth rate of 0.44 mm/s and a temperature gradient of 0.34 K/mm. That critical cooling rate was quite close to the 0.2 K/s found earlier for Al-Cu alloys (Ref 15). The columnar-equiaxed transition in Sn-Pb alloys (Ref 19) was observed at cooling rates higher than this critical value.

The morphology transition of Al-3 wt.% Si was observed using unsteady-state horizontal directional solidification (Ref 20). The transition was sharp and occurred along a plane parallel to the chill wall because of the high density of rapidly growing equiaxed grains. It was observed for a tip growth rate of about 0.26 mm/s, a temperature gradient in the melt of about 0.44 K/mm, and a tip cooling rate of 1.68 K/mm.

The effect of Si content on the columnar-to-equiaxed transition was studied in Ref 13 using upward unsteady-state unidirectional solidification of aluminum-based alloys with 5.5, 7.5 and 9 wt.% Si and 3 wt.% Cu. The positions of the transitions in the mold depended on Si concentration, unlike in the observations of (Ref 14). The transition occurred for tip growth rates from 0.25 to 0.63 mm/s and a temperature gradient in the melt ahead of the liquidus isotherm ranging from 1.95 to 4.24 K/mm. Therefore, the criterion of the transition cannot be determined by only one particular thermal parameter. It has to encompass the tip growth rate V , the temperature gradient G and the cooling rate $T_R = V \times G$ (Ref 21). The critical value of the transformation depended on the alloy system and was about 1.17 K/s for the alloys studied (Ref 13).

2.2.2 Hypoeutectic Alloys. Hypoeutectic Al-Si alloys usually have a dendritic morphology (Ref 5, 22). A dendritic microstructure is characterized by the primary dendrite arm spacing λ_1 , secondary dendrite arm spacing λ_2 , dendrite tip radius R and, in several papers, the mushy zone depth d . These parameters are functions of the temperature gradient G ahead of the microscopic solidification front and the growth rate V (Ref 23-32). Several theoretical models of the formation of a dendritic microstructure were developed at the end of the last century (Ref 33-41). Experimental investigations of the V and G dependence of microstructure parameters had been performed for directional solidification of alloys at both steady-state and unsteady-state conditions. In Ref 42, Al-3 wt.% Si alloys were grown by the Bridgman method under steady-state conditions either with a constant growth rate of $8.20 \mu\text{m/s}$ and a temperature gradient ranging from 1.97 to 6.84 K/mm, or with a constant temperature gradient of 6.84 K/mm and growth rates from 8.20 to $492.76 \mu\text{m/s}$. The following microstructure parameter dependences on V and G were $(\lambda_1, \lambda_2, R, d) = k_i G^{-ai}$

at constant V and $(\lambda_1, \lambda_2, R, d) = kV^{-b_i}$ at constant G . Here, k_i is the proportionality constant for the i th parameter, while a_i and b_i are the corresponding exponents for temperature gradient and growth rate, respectively.

The average values of λ_1, λ_2, R and d for an alloy of constant Si content for different G and constant V were $-0.47, -0.58, -0.59$ and -0.89 . The average values for the same parameters in the case of different V and constant G were $-0.28, -0.47, -0.45, -0.38$. The experimental values of λ_1, λ_2, R and d decreased as V increased at constant G and they decreased as G increased at constant V . The dependence of these parameters on G was stronger than on V .

For the most part, (Ref 42) reported good agreement of the exponent values for λ_1, λ_2, R and d for Al-3 wt.% Si alloys with the values of previous works for different alloy systems. There were references to 27 papers. Here, we describe only the results for references from this century (Ref 14, 21, 43, 44). These studies were performed with unsteady-state directional solidification as opposed to steady state as in Ref 42.

In Ref 42, the experimental dependence of λ_1, λ_2, R and d on growth parameters V and G was compared with theoretically predicted behavior. Trivedi Ref 37 obtained the following equation:

$$\lambda_1 = 2.83\{m(k-1)D\Gamma L\}^{0.25} C_0^{0.25} V^{-0.25} G^{-0.5}, \quad (\text{Eq 1})$$

where m is the liquidus slope, k the partition coefficient, D the diffusion coefficient, Γ the Gibbs–Thomson coefficient, C_0 the solute content and L is a constant that depends on a harmonic perturbation. An identical dependence of λ_1 on solidification parameters was obtained by Hunt Ref 35, Kurz and Fisher Ref 36, the difference between them being only the value of the constant. Experimental λ_1 values agreed very well with those calculated using Eq 1. The λ_2 values calculated using the Trivedi–Somboonsuk model Ref 39 were in very good agreement with experimental values. There was also good agreement of the Trivedi model (Ref 37) with experiment values for R . Other models (Ref 33–36, 38) described behavior adequately only for individual microstructural parameters or in separate ranges of V and G .

Microstructural investigations for Al alloys containing 3, 5, 7 and 9 wt.% Si were performed with samples obtained by directional solidification under upward unsteady-state conditions (Ref 14). A combined theoretical and experimental approach was developed to quantitatively determine tip growth rate, temperature gradient, tip cooling rate and other parameters. The rate dependence of λ_1 and λ_2 is shown in Fig. 3 (Ref 14, 42) and 4 (Ref 14), respectively. The primary dendrite arm spacing is described as a -0.55 -power dependence on tip cooling rate T_R . The silicon concentration C_0 in the range studied did not influence λ_1 . The secondary spacing λ_2 decreased as the solute content increased according to a $-2/3$ power law. The spacing λ_2 decreased as C_0 increased. Such a dependence of λ_1 on T_R had been observed for Sn-Pb and Al-Cu alloys (Ref 45). Results for the effect of C_0 on λ_1 showed contradictions. A small effect of C_0 on λ_1 was observed for Al-Cu alloys both for steady-state (Ref 32) and for unsteady-state directional solidification (Ref 45). For Sn-Pb alloys directionally solidified under unsteady-state heat flow conditions, λ_1 decreased when C_0 increased (Ref 45). Most of the results from the literature for λ_2 also show a decrease in secondary spacing with increasing C_0 . In Ref 14, it was observed that among the published theoretical models only those proposed by Hunt and

Lu (Ref 33) for primary spacing and Bouchard-Kirkaldy 38 for primary and secondary spacings account for unsteady-state heat flow conditions during solidification. The scatter of experimental values of dendritic primary spacing λ_1 as a function of cooling parameter $G^{-0.5}V^{-0.25}$ (Ref 14) is included inside the range of minimum and maximum values predicted by the Hunt-Lu model. Predictions made using the Bouchard-Kirkaldy model are generally slightly above the experimental points.

The microstructure of aluminum alloys obtained by horizontal directional solidification with unsteady-state heat flow conditions was investigated for Al-3 wt.% Si (Ref 20) and Al-7 wt.% Si (Ref 46). In both works, the primary dendrite arm spacing increased when either the growth rate or the cooling rate was decreased. The primary dendritic arm spacing depended on the tip growth rate according to the power law $\lambda_1 = \text{constant } V^{-1.1}$. The dependence of arm spacing on cooling rate was given by $\lambda_1 = \text{constant } (T_R)^{-0.55}$. This is in agreement with Ref 14, 44 for Al-Si and with Ref 45 for Sn-Pb and Al-Cu. Good agreement with theory Ref 33, 38 was observed in Ref 46 for Al-7wt. % Si, but the authors (Ref 20) noted some differences for Al-3 wt.% Si.

2.2.3 Near-Eutectic Alloys. The influence of solidification rate on the microstructure of near-eutectic Al-Si alloys was studied for rates from 1.7×10^3 to $8.3 \times 10^3 \mu\text{m/s}$ (Ref 47). Al-11.3 wt.% Si alloy was cast into rods using a horizontal continuous casting process with a heated mold (Ref 48, 49). The microstructure, referred to as feathery grains or twinned crystals, has often been observed in aluminum and aluminum alloys prepared by continuous casting. Factors favoring the formation of these feathery grains have been noted (Ref 47) as a high G (temperature gradient in the mushy zone) and high solidification rate. The directionality of the microstructure increased as the solidification rate increased. The area fraction of dendrites in the longitudinal section increased with an increase in the solidification rate. This effect was attributed in Ref 47 to a shift in the composition for eutectic solidification (coupled growth) to higher Si levels and a lower temperature. This can be seen in Fig. 1, where the points on line 7 show the compositions and the solidification rates of the alloys studied in this work. Note that increasing the solidification rate to $8.3 \times 10^3 \mu\text{m/s}$ caused the Si content to become much less, 11.3 wt.%, than that required for coupled growth represented by line 2 in Fig. 1.

The dependence of the microstructure for alloys of constant composition on the solidification rate was determined in several works. For example, such studies were performed from 20 to $400 \mu\text{m/s}$ (Ref 50), 0.1 to 500 (Ref 51), 28 to 875 (Ref 52), 300 to 790 (Ref 53), 10 to 1218 (Ref 10) and 10 to 2000 $\mu\text{m/s}$ (Ref 54). A complete list of papers on this subject was given in Ref 54. As a rule, the character of the eutectic microstructure was described by the average spacing between flake and fiber of Si phase:

$$\lambda = (1/M)(A/N)^{1/2}, \quad (\text{Eq 2})$$

where N is the number of silicon of particles in a known area A of a section at magnification M . The mean spacing between approximately parallel flakes λ_f and the random line spacing λ_L was calculated. The value of λ_L was determined using the intersections of lines oriented randomly with flakes. In the above-mentioned papers, both spacings followed the relationship:

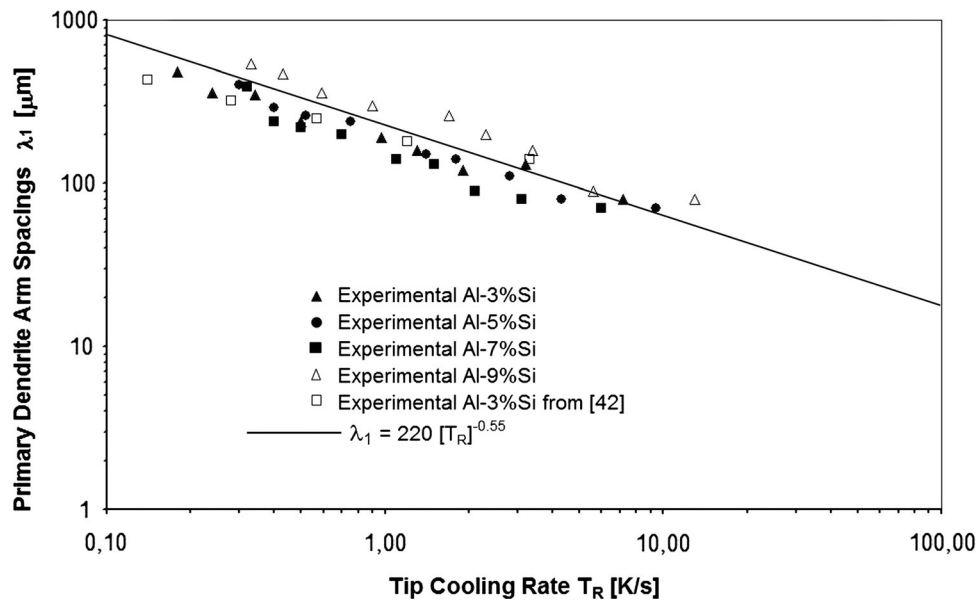


Fig. 3 Primary dendrite arm spacing as a function of the cooling rate for Al-Si alloys in Ref 14 and in Ref 42 (white squares)

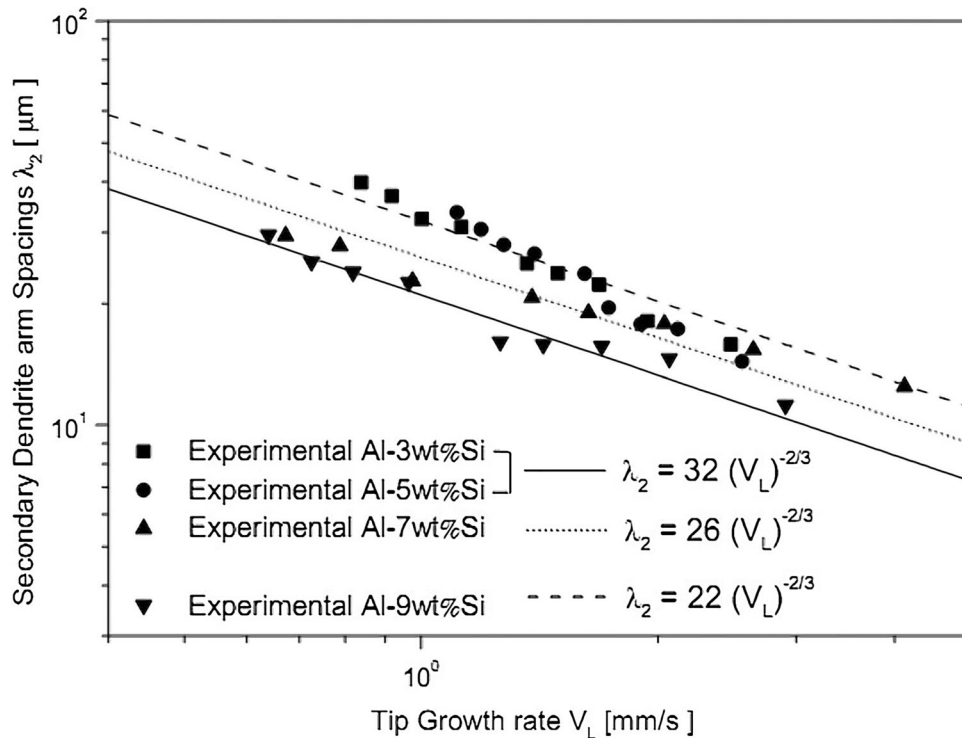


Fig. 4 Secondary dendrite arm spacing as a function of growth rate for Al-Si alloys (Ref 14)

$$\lambda = AV^m, \quad (\text{Eq 3})$$

where m varied from -0.3 to -0.6 . Figure 5 shows the dependence of average spacing parameters on freezing rate for all of the papers cited above. In the majority of works, $m = -0.5$. Different values of m can be attributed to different cooling rates. The average particle aspect ratio, c/a , was also used as an additional spacing metric in Ref 54, as shown in Fig. 5. Here c is the longest distance across a particle in cross section and a is the distance between parallel tangents. Note that only the

average particle aspect ratio has three regions of different c/a behavior. This spacing metric seems to show a morphological transition. Really from 10 to about 135 $\mu\text{m/s}$, flakes in the eutectic were dominant. The morphological transition took place from 135 to 880 $\mu\text{m/s}$. Qualitative analysis of the morphology was performed using scanning electron microscopy. This showed that the plate morphology decreased significantly at a solidification rate from 100 to 250 $\mu\text{m/s}$. The growth of rod-like structures within the plane of the plates was

noted. At 500 $\mu\text{m/s}$, rods began to grow out of flat plate faces. At 950 $\mu\text{m/s}$, fibrous rod growth was dominant (Ref 54).

2.2.4 Hypereutectic Alloys. The mechanical properties of hypereutectic alloys depend on the microstructure of both the eutectic matrix and the primary silicon crystals. The morphology of these structures depends on many factors: the superheat of the bulk melt, the undercooling of the melt ahead of the solid-liquid interface, the growth rate and the alloy composition, including the type and amount of any modifier, alloying additions and impurities. The different characters of silicon microstructure of hypereutectic Al-Si alloys obtained by vertical Bridgman directional solidification are shown in Fig. 6 (Ref 10).

The effect of undercooling on the morphology of primary and eutectic silicon of hypereutectic Al-Si alloys with various Si content was studied in Ref 55. To obtain large undercooling, they produced droplets of the alloy in a molten salt by the droplet emulsion technique. The microstructure of alloys with 18, 20 and 25 wt.% Si solidified at various undercoolings was studied by scanning electron microscopy. Based on these results, microstructure selection maps of primary and eutectic Si were built (Fig. 7). It is seen that the critical level of undercooling for the morphological transition from star-like to massive Si increases with the increasing silicon content.

Review (Ref 56) described six basic shapes of primary silicon and attempts to find mechanisms for their growth. Here, we describe only the conditions for their nucleation.

Star-like primary silicon crystals were observed at low growth velocities (Ref 10). Often the star-like silicon crystals in hypereutectic Al-Si alloys have a unique fivefold symmetry of quasicrystals, as shown in Fig. 6 from (Ref 10). The nucleation and growth of star-like silicon depend on the undercooling and solidification rate (Ref 57). These processes occur within the undercooled melt ahead of the solidification interface (Ref 58, 59). The combination of undercooling and composition yielding this morphology was revealed in Ref 55 as shown in Fig. 7.

The *feathery* silicon morphology shown in Fig. 6(c) is from (Ref 10). According to Ref 55, superheating the melt above

850 $^{\circ}\text{C}$ leads to cluster formation and the complex structure of the alloy. This morphology is sometimes called *fishbone*.

Polyhedral primary silicon crystals are mainly found in hypereutectic Al-Si alloys inoculated with phosphorous (Ref 56). The morphology of primary silicon crystals of Al-18% Si depends on the growth rate, temperature gradient and cooling rate (Ref 60). At a cooling rate of 2.0 K/s, the primary silicon is polyhedral. The nucleation of such morphology depends on the contact angle between liquid and solid phases, which is a function of the cooling rate. It was found that the effective angle for heterogeneous nucleation of polyhedral primary particles is $30^{\circ} \pm 4^{\circ}$, which occurs in the presence of phosphorus at slow solidification rates. It appears that AlP decreases the nucleation energy of polyhedral particles. Rapid cooling (Ref 61, 62) and superheating (Ref 63) have been considered as methods to change the size of the primary silicon. The effect of the liquid structure before solidification on the microstructure of silicon in Al-Si hypereutectic alloy and the effect of cooling rate and superheating treatment on the size (Ref 61, 64) and morphology (Ref 65) of primary silicon were studied. It was found that with an increase in the superheating of the melt, the size of primary silicon decreased and the shape of the primary silicon crystals changed from star-like and other irregular shapes to octahedral. This can be explained by the formation of nuclei of star-like and other irregular primary silicon from Si-Si clusters of larger size, and formation of nuclei of octahedral silicon from Si-Si clusters of smaller sizes. The effect of melt superheating on the size and morphology of primary silicon is shown in Fig. 8. It is worth noting that sections of octahedral primary silicon in SEM micrographs have different polygonal outlines; triangular, square, trapezoidal, hexagonal (Ref 66). According to Ref 65, the size of primary silicon particles decreases, but the shape of the crystals does not change with increasing cooling rate, provided that the cooling rate is lower than a critical rate. The cooling rate affects the morphology of primary silicon crystals if it is higher than 37.5 $^{\circ}\text{C/s}$. However, the exact value of the critical rate was not determined.

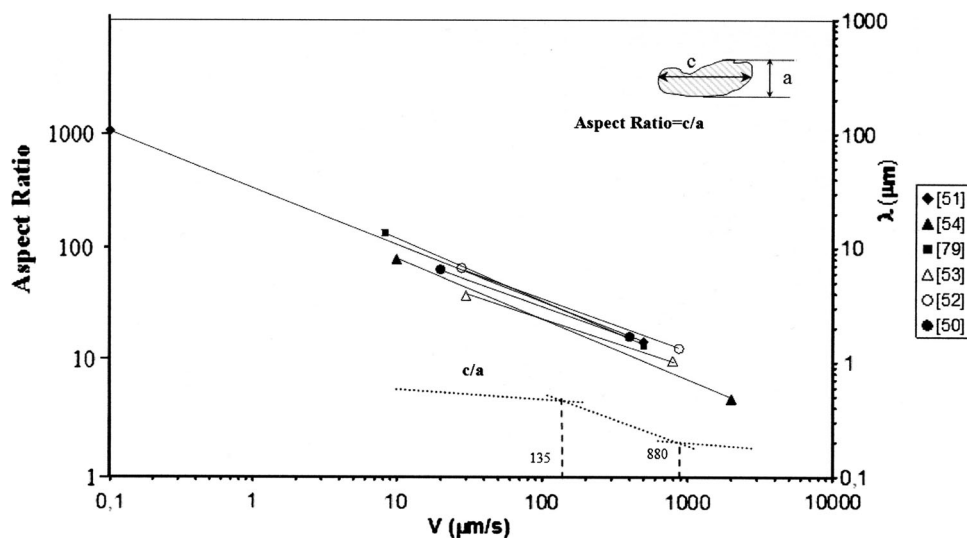


Fig. 5 General schematic diagram of average spacing and the average particle aspect ratio versus solidification rate according to Ref 50-54. The aspect ratio in Ref 54 displays distinct transition points near 135 and 880 $\mu\text{m/s}$, which are near the visually observed onset and conclusion of the flake-to-fiber transition

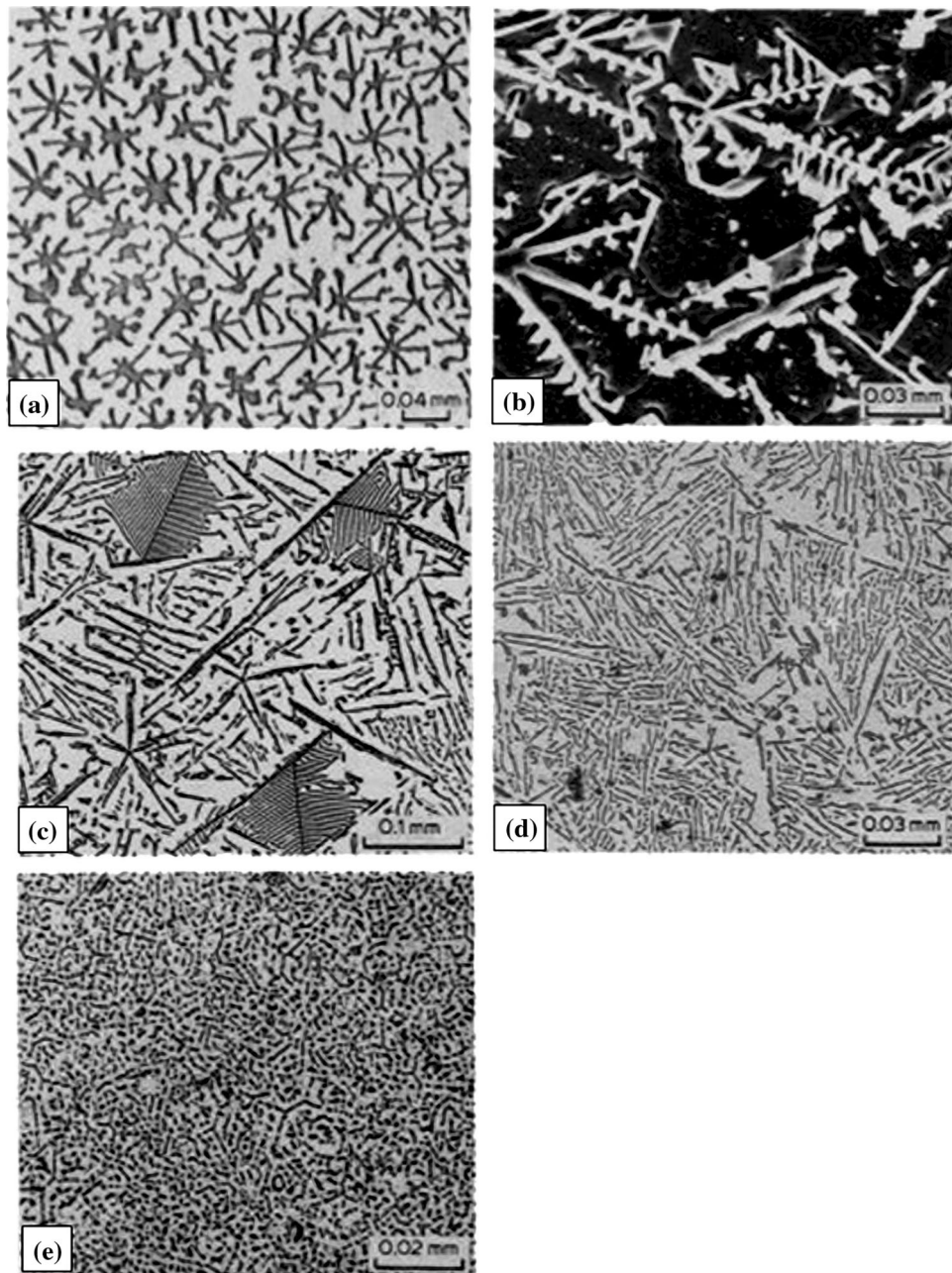


Fig. 6 Dependence of microstructure in a transverse section on the solidification rate. (a) Angular silicon crystals developed from silicon rods, Al-15 wt.% Si alloy, growth velocity of $1.5 \mu\text{m/s}$. (b) Complex regular lamellae on angular silicon side plates in an Al-15 wt.% Si alloy, growth rate of $1.8 \mu\text{m/s}$. (c) Flake eutectic, complex regular and star-like silicon of Al-15.75 wt.% Si alloy, growth rate of $10 \mu\text{m/s}$. (d) Flake eutectic of Al-15 wt.% Si alloy, growth rate of $100 \mu\text{m/s}$. (e) Angular silicon and fibrous eutectic of Al-17 wt.% Si-0.048 wt.% Sr alloy, growth rate of $100 \mu\text{m/s}$ (Ref 10)

Dendritic primary silicon crystals are formed in hypereutectic Al-Si alloys due to Sr additives or small undercooling of the melt (Ref 56). In Ref 67, the effect of Sr in the concentration range 0-0.1 wt.% on the structure of Al-Si alloys containing 11-20 wt.% Si and solidified from 1 to $1500 \mu\text{m/s}$ with a temperature gradient of $12.5 \text{ }^\circ\text{C/mm}$ was studied. Small Sr additions seemed to poison sites for layer growth, causing holes, branching and formation of dendritic primary Si crystals. Larger amounts of Sr increased the dispersed equiaxed structure. Sr broadened the coupled zone of solidification and changed the anomalous Si flake eutectic to a fibrous structure.

The effect of undercooling from 10 to 320 K on the morphology of Al-50 at.% Si alloy was investigated in Ref 68. Levitated droplets were frozen with a helium gas flow. At small undercooling, the primary silicon had faceted dendrites with second-, third-, and higher-order branches (Fig. 9 and 10). When the undercooling was increased to 70 K, the network of plate-like crystals had more diverse branching. At a large undercooling of 320 K granular primary crystals of 10 to $20 \mu\text{m}$ in diameter were observed.

The *spheroidal structure* of primary silicon was long known to arise with sodium additions. In an Al-20 wt.% Si alloy of

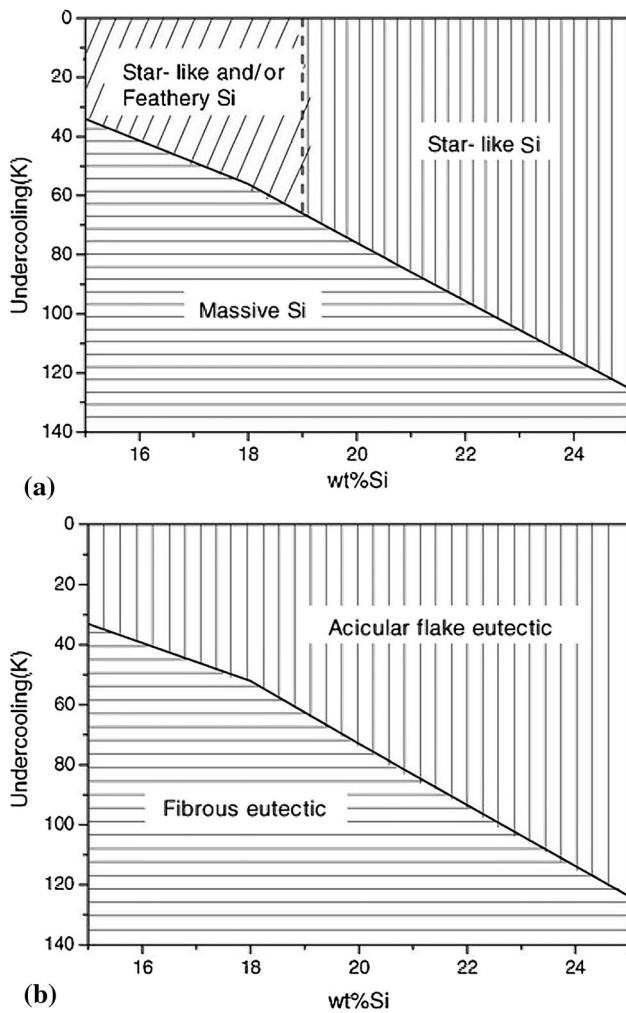


Fig. 7 Microstructure selection maps of hypereutectic Al-Si alloys (SEM image): (a) primary Si, (b) eutectic Si (Ref 55)

high purity containing sodium, idiomorphic faceted crystals of primary silicon with a few twins were found (Ref 69). A modification of the eutectic phase occurred with small sodium additions (150 ppm). Larger additions (230-1000 ppm) caused a modification of primary crystals to a round shape with a high twin density. With 0.5 wt.% Na added, the primary silicon crystals had a spherical shape and consisted of a few interpenetrating twins. The twin density increased with addition of more Na. An explanation (Ref 70) of the mechanism of formation of a spheroidal structure with variations in composition and temperature was made possible by investigating the structure of both equiaxed faceted crystals (Ref 71) and the most familiar plate-like silicon crystals (Ref 72). When hypereutectic Al-Si alloy was over-modified by Na, roughly spherical primary silicon crystals formed (Ref 71, 73). Spheroidal silicon crystals consisted of several pyramidal silicon grains with their apices at the center of the sphere. The surfaces of these spheroids were faceted (Ref 71), mostly with $\{111\}$ planes. Some facets were also parallel to the less densely packed $\{100\}$ and $\{211\}$ planes. Sodium was concentrated at the grain boundaries. A limited number of these grains were twin-related. It was proposed (Ref 70, 74) that the nucleus for the growth of spherical silicon crystal is a decahedron formed by five silicon tetrahedra pre-existing in the melt. An

equiaxed crystallite grows because its surface is mostly $\{111\}$ planes with lower surface energy than the faces of an idiomorphic single crystal. With the growth of a spherical crystallite, the ratio of surface-to-volume decreases. This leads to a decrease in the energy advantage, resulting in an increase in the instability of the growth. With anisotropy in the growth rate, there is also the possibility of formation of planes less close packed than $\{111\}$. Also, if some twinning takes place then the twin plane reentrant edge (TPRE) mechanism can operate and change the growth mode (Ref 5). The latter does not happen because the process is inhibited by sodium. So, the spherical crystallite is forced into isotropic growth, but the minimum energy of the liquid-solid interface is maintained when the surface consists mostly of $\{111\}$ planes (Ref 70).

Flat plate primary silicon crystals nucleate as aggregates of silicon tetrahedra pre-existing in the melt (Ref 70). The shape of a subsequent crystal depends on the number of aggregated tetrahedra, Fig. 11. For example, a combination of two tetrahedra (Fig. 11a) can lead to the growth of a flat plate. The growth of this combination to form the nearly spherical form in Fig. 11(b) is energetically more favorable than that of Fig. 11(a). During the growth of the nucleus to a critical size, the combination of two or more $\{111\}$ plates can form a twin plane reentrant edge. In that case, growth in the $\langle 211 \rangle$ direction is much faster than in the $\langle 111 \rangle$ direction. The crystal then grows into a flat plane with $\{111\}$ faces.

3. Mechanical Properties

The mechanical properties of Al-Si alloys obtained by conventional casting have been investigated rather widely. There has been less study of directionally solidified alloys. The background for the results of directional solidification investigations is given in this chapter. There are references to reviews on the structure and mechanical properties of the alloys: (in 3.2.2:—Hegde and Prabhu 2008; in 3.2.3:—Sigworth 2008) and earlier in Ref 56.

3.1 Elasticity and Hardness

Studies of the effect of silicon content on Young's modulus of Al-Si alloys were performed over a wide range of Si concentrations on samples obtained by two methods. Casting of a levitated melt with an estimated solidification rate of about $5 \times 10^3 \mu\text{m/s}$ was used in Ref 6. Levitation of Al-Si melts was achieved by an alternating inhomogeneous magnetic field. A generator of 300-600 kHz and 10 kW power was used to create the field. The liquid metal was cast into a massive Cu mold by decreasing the inductor voltage. The melting and the casting were carried out in a helium atmosphere of 10^5 Pa pressure. In Ref 7, 75, samples were prepared by directional solidification using Stepanov's method (Ref 8) at rates up to $10^3 \mu\text{m/s}$. An increase in the Si content in Al-Si alloys resulted in a nearly linear decreasing density ρ (Fig. 12) and an increasing Young's modulus E (Fig. 3 in Ref 6).

The temperature dependence of Young's modulus of alloys with various Si contents was studied in Ref 6. It was revealed that the Si content had a significant effect on the decrease rate of Young's modulus with increasing temperature to 500 °C (Fig. 4 in Ref 6). The Si concentration dependence of the average temperature coefficient of Young's modulus, $\Delta E/$

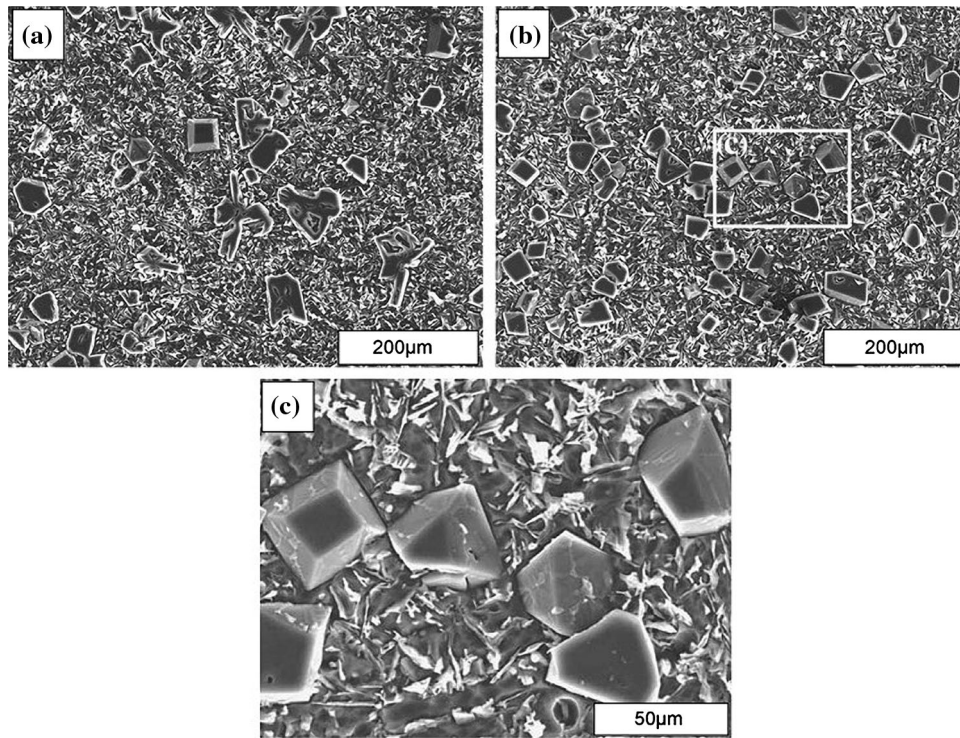


Fig. 8 SEM micrographs of Al-20 wt.% Si alloy: (a) with a pouring temperature of 850 °C, (b) with a pouring temperature of 1050 °C and (c) magnified picture of the indicated region in (b) (Ref 65)

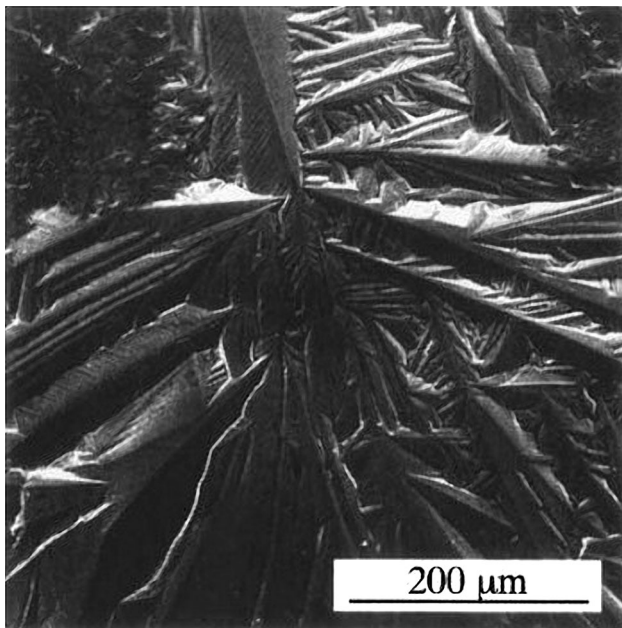


Fig. 9 Scanning electron micrograph of the surface morphology of a 10-mm Al-50 at.% Si droplet solidified at an onset undercooling of 10 K (Ref 68)

($E_{20}\Delta T$), while cooling from 500 to 20 °C had maximum at 20 wt.% Si. Here ΔE is the change of Young's modulus in temperature range ΔT , E_{20} is E at 20 °C. The hysteresis in Young's modulus at 20 °C, $E_{20}/\Delta E_{20}$ from measurements of the temperature dependence of E had been shown in Ref 6.

The extremums at about 20 wt.% Si can be explained by the coupled growth of the eutectic microstructure at a solidification

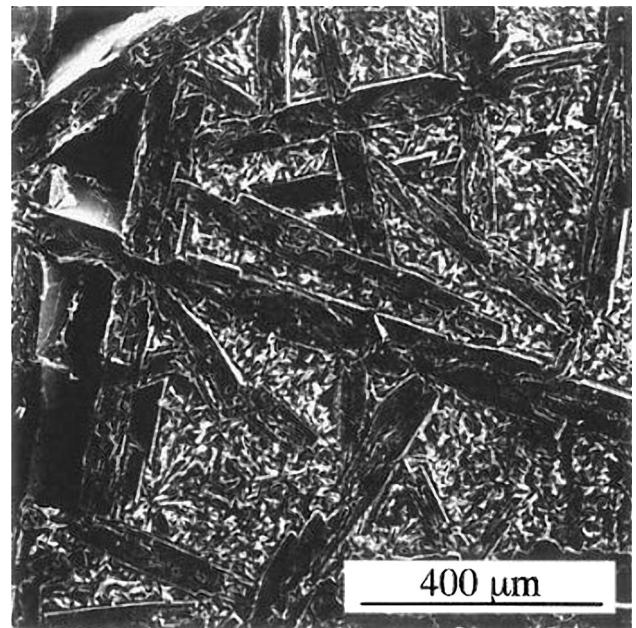


Fig. 10 Scanning electron micrograph of a polished and deeply etched section of droplet solidified at an onset undercooling of 10 K. The etching had removed the aluminum, leaving the morphology of the silicon clearly visible (Ref 68)

rate of about $5 \times 10^3 \mu\text{m/s}$. The yield point of these alloys was measured by three-point bending of samples 20 mm in length and $1.6 \times 2.5 \text{ mm}^2$ in cross section at a constant bending rate of about $0.5 \mu\text{m/s}$. As shown in Fig. 13, the load P corresponding to the yield point also exhibited a maximum at about

20 wt.% Si, corresponding to a eutectic microstructure without any primary crystals.

The microhardness of the α -Al solid solution was analyzed in detail for the first time in Ref 76. It was shown that the microhardness of the α -Al solid solution in homogeneous alloys became constant when the silicon content reached saturation. However, in some works, a Si content dependence of microhardness was observed. This was attributed to inhomogeneity of the solid solution connected with features of the method of crystallization (Ref 6).

The microhardness of Al-Si alloys obtained by solidification using Stepanov's technique (Ref 8) at a constant rate of $10^3 \mu\text{m/s}$ was studied in Ref 7. It was shown (Fig. 14) that at an indentation load of 10 g, the Vickers microhardness of the coupled α -Al + Si microstructure did not depend on the silicon content in the investigated range of 8 to 25 wt.% Si. This result confirmed that the eutectic structure of the alloy obtained at a constant solidification rate is independent of the silicon concentration.

The Vickers microhardness of Al-Ge alloys of various Ge content was measured to make sure that the above result is valid for all eutectic-forming aluminum alloys with limited solid solubility of the components (Ref 75). Samples were obtained by solidification using Stepanov's technique at a solidification rate $10^2 \mu\text{m/s}$. The Ge content was 35, 43, 53, 57 and 64 wt.%

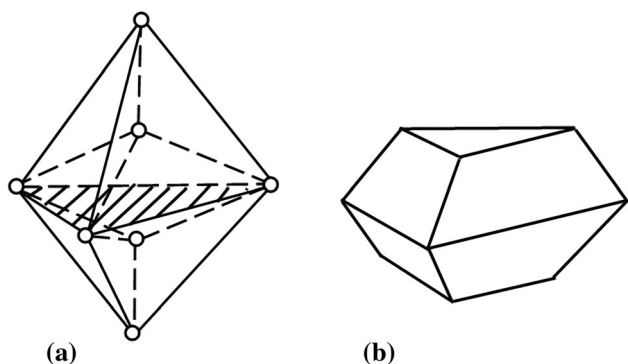


Fig. 11 (a) Silicon tetrahedra with $\{111\}$ mirror plane (shaded); (b) Truncated tetrahedra at later stage growth (Ref 70)

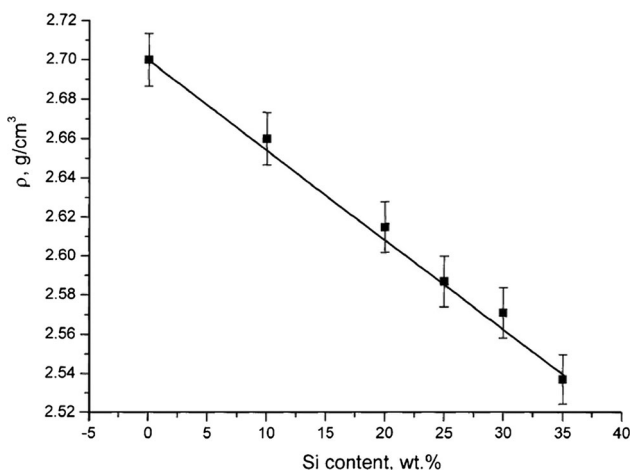


Fig. 12 Density of Al-Si alloys as a function of Si content (Ref 6)

Ge. The equilibrium eutectic point of Al-Ge is about 52 wt.% Ge (Ref 4). Again, the Vickers microhardness did not depend on Ge content at constant solidification rate (Fig. 14).

At the end of the last century, several authors studied the possibility of using hardness measurements to estimate the yield strength or tensile strength of eutectic Al-Si alloys. In Ref 77-79, the mechanical properties of 12.6 wt.% Si alloys were considered in terms of the behavior of composite materials. The yield strength varied according to:

$$\sigma_y = \sigma_0 + K_y \lambda^{-1/2}, \quad (\text{Eq 4})$$

where σ_0 and K_y are the friction stress and a constant, respectively; the lamellar spacing λ appears similar to the grain size d in a Petch-Hall relationship for polycrystalline materials. If $\lambda \propto V^{-1/2}$ (Ref see expression (3) of section 2.2.2)) then it follows that:

$$\sigma_y \propto V^{1/4}. \quad (\text{Eq 5})$$

In Al-Si alloys, the hardness H and freezing rate V are related for a fixed temperature gradient by the Eq 4:

$$H = H_0 + K_v V^a \quad (\text{Eq 6})$$

According to Ref 78, the exponent a is equal to 0.09 and 0.11 for longitudinal and transverse sections, respectively. The dependence of hardness H on interflake spacing λ is

$$H = H_0 + k \lambda^{-b} \quad (\text{Eq 7})$$

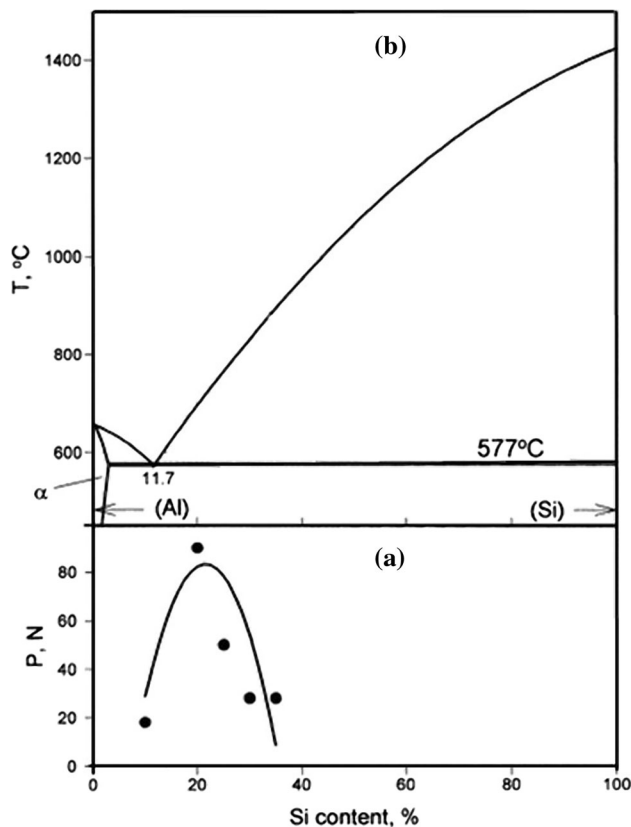


Fig. 13 (a) The yield point P as a function of Si content; (b) The aluminum-silicon phase diagram (Si content in wt.%) (Ref 6)

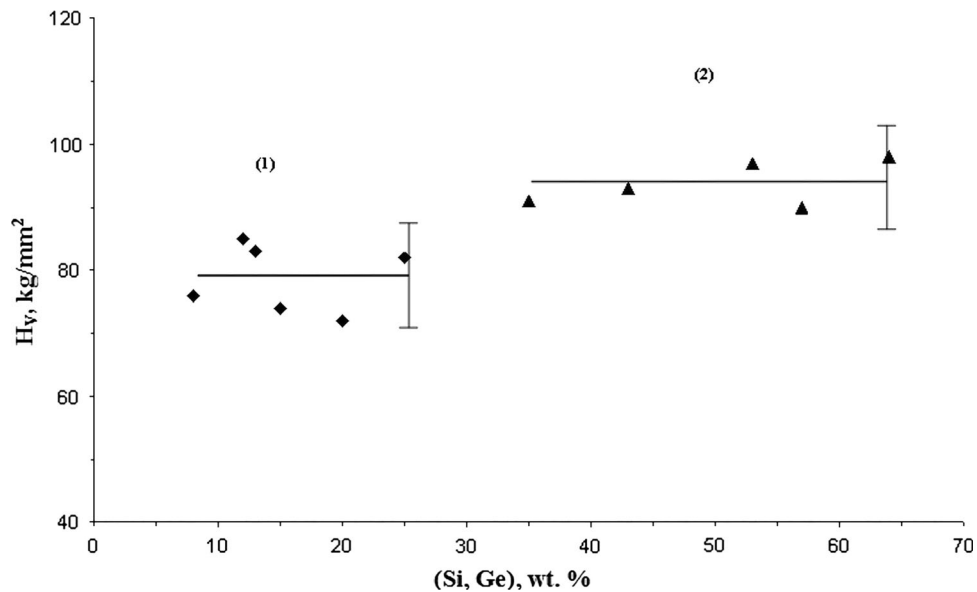


Fig. 14 Dependence of the Vickers microhardness at a load of 10 g for: (1) the eutectic microstructure vs. Si content (Ref 7); (2) the eutectic vs. Ge content (Ref 75)

The value of b at a temperature gradient of 7.8 K/mm is 0.16 and 0.18 for longitudinal and transverse sections, respectively (Ref 78). The last value is in good agreement with 0.22 found in Ref 79 and somewhat higher than 0.08 given in Ref 10. The good agreement of the dependence of H_v on V from different works (Ref 7, 10, 77, 79-82) is shown in Fig. 15. Data of work (Ref 83) are also included in Fig. 15. The Vickers hardness as a function of growth rate V (Ref 83) does not obey Eq 6. This may be connected with the use of an indenter load of 2.5 kg rather than the 10-25 g usually used. The resulting indentation might include not only a eutectic microstructure but also primary α -Al crystals. The lower hardness and sharper increase of hardness observed in Ref 83 at a solidification rate of about 500 $\mu\text{m/s}$ can be explained in the same way.

In Ref 10, the effect of eutectic silicon microstructures on the exponents in H expressions (6) and (7) was emphasized. The exponent b in (7) was equal to 0.5 for the angular silicon morphology, and equal to 0.08 for the flake, fibrous and complex regular silicon morphologies. A similar dependence of the yield strength σ_y on spacing λ was found in Ref 77, 78 for flake eutectic silicon. The Hall-Petch dependence of σ_y and H on λ with an exponent of 1/2 was found in Ref 81 for the flake silicon, unlike in Ref 10 where $b = 0.5$ only for the angular morphology. A more complex relationship between H and V was observed for hypereutectic compositions, 15-17 wt.% Si (Ref 10). It is conceivable that an analysis of a relationship between H and V for such alloys has to use the planar-volume method in considering the structural transformation of eutectic silicon developed in Ref 53.

It is also necessary to note the investigation of Vickers hardness (Ref 83) as well as tensile and compressive properties of Al-Si over a wide range of growth rates from 2.8×10^{-1} to $10^4 \mu\text{m/s}$. It was found that there was no correlation between hardness and strength over the entire range of growth rates. Similar trends were seen between hardness and compressive yield strength. Therefore, the question of the possibility of control of the strength of Al-Si alloys based on hardness remains open.

3.2 Plasticity and Strength

3.2.1 Silicon Concentration Effect. The strength of cast binary Al-Si alloys has been studied only in recent decades, especially for directional solidification over a wide range of silicon content. According to Fig. 16 (Ref 84), based on the data of Ref 85, for samples obtained by casting into sand or a mold the ultimate tensile strength (UTS) σ_B increased with Si content in hypoeutectic alloys and decreased in hypereutectic alloys. The value of σ_B resulting from casting into the sand was lower than for casting into a mold because the solidification rate in the sand is lower than in a mold. In Ref 84, it was noted that there was not a general model explaining the strength behavior of Al-Si alloy. It is possible to suppose that an increase of σ_B with Si content up to the composition for coupled growth of a eutectic microstructure is determined mainly by the increase in relative volume fraction of the stronger microstructure compared to α -Al. The increase in strength caused by increasing the solidification rate can be explained by the resulting increase in dispersion of the eutectic microstructure and a decrease in silicon particle spacing, hindering the movement of dislocations. But it is unclear why the maximum of strength curves in Fig. 16 for a mold corresponded to a lower Si content than for sand. It was well known (Ref 5) that an increase in the solidification rate as well as chemical modification leads to an increase in undercooling of the melt near the liquid-solid interface.

Investigations at solidification rates of about 10^2 , 10^3 and $5 \times 10^3 \mu\text{m/s}$ showed that the UTS of Al-Si alloys corresponded to the growth of a eutectic microstructure (Ref 6, 7). As the freezing rate increased, the UTS increased toward higher Si content along with the composition for eutectic growth. Figure 17 shows the tensile stress-strain diagram of Al-Si for various silicon concentrations directionally solidified at $10^3 \mu\text{m/s}$ using Stepanov's method. The ultimate tensile strength increased with increasing silicon content up to about 15 wt.%, followed by a sharp decrease with additional Si. At the same time, the fracture elongation decreased with increasing

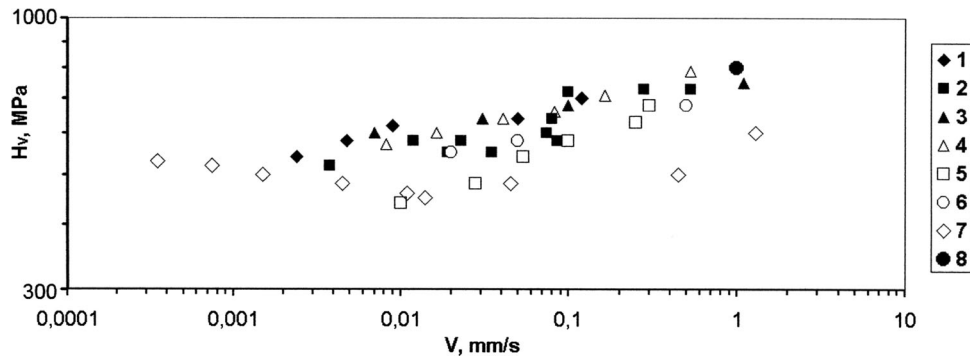


Fig. 15 Comparison of H_v as a function on the solidification rate V on data of different works (in Ref 79 (1-6), (Ref 83)-7 and (Ref 7)-8)

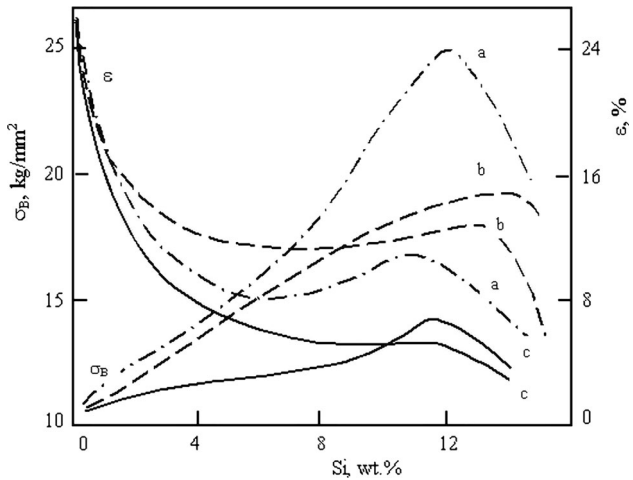


Fig. 16 Influence of Si content on the tensile strength and fracture elongation of Al-Si alloy obtained by casting into a mold (a) and into sand with sodium modification (b) and without modification (c) (Ref 84)

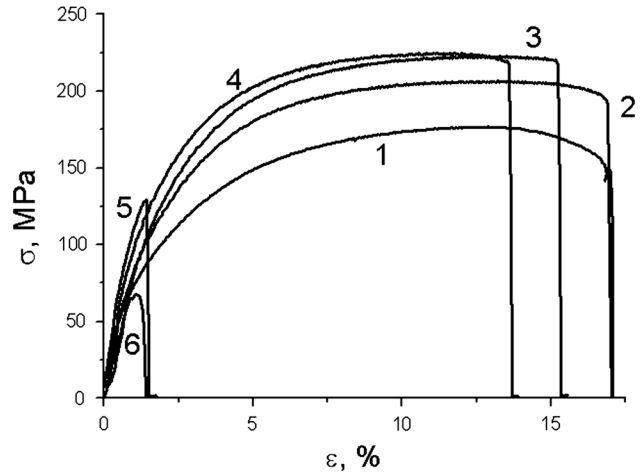


Fig. 17 Stress-strain tensile diagrams of Al-Si alloys containing (1) – 8, (2) – 11.7, (3) – 13, (4) – 15, (5) – 20, and (6) – 25 wt.% Si (Ref 7)

Si content, particularly beyond the composition giving a eutectic microstructure.

Figure 18 shows the silicon concentration dependence of the UTS and the yield strength at 0.2% strain. The UTS at a solidification rate of $10^3 \mu\text{m/s}$ was observed at 15 wt.% Si, where the microstructure of the alloy was eutectic without primary crystals of either $\alpha\text{-Al}$ or Si (see Fig. 2). Thus, it is possible to consider the composition giving a eutectic microstructure as the point of the ductile-to-brittle transition. The transition can be explained as a change in the fracture mode at the change in microstructure. Hypoeutectic alloys with Si content up to the limit of coupled eutectic growth without any primary crystals can be considered as a composite: the $\alpha\text{-Al}$ solid solution is plastic while the eutectic microstructure is brittle.

The dependence of UTS (σ_B) on Si content can be described by the mixture law:

$$\sigma_B = \sigma_\alpha V_\alpha + \sigma_e V_e, \quad (\text{Eq 8})$$

where V_α is the volume fraction of the primary dendrite crystals of $\alpha\text{-Al}$ and $V_e = 1 - V_\alpha$ is the fraction with a eutectic microstructure. At low freezing rates, the volume fractions can be found from the phase diagram using the lever rule. The value σ_α is equal to σ_B of the dendritic crystals of the $\alpha\text{-Al}$ solid

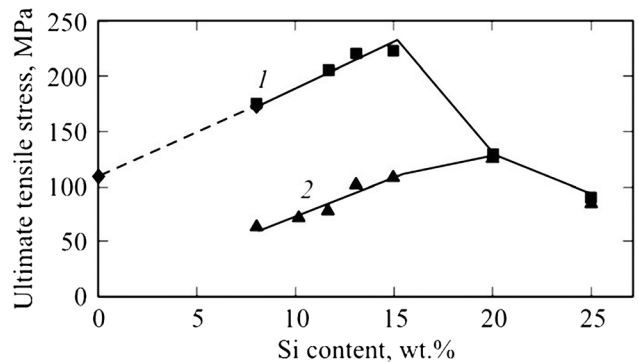


Fig. 18 Dependences on Si content of the ultimate tensile strength and the yield strength at a relative elongation of 0.2%. (1)—UTS, the dashed line is an extrapolation from 8 to 1.6 wt.% Si; (2)—yield strength

solution. It can be found by extrapolation of the experimental dependence of σ_B on the Si concentration to the limiting saturation concentration of $\alpha\text{-Al}$ solid solution. The value σ_e is the UTS, σ_B of the eutectic structure (for 15 wt.% Si). The calculated dependence of σ_B on the Si content is shown in Fig. 18 for $\sigma_\alpha = 110 \text{ MPa}$ and $\sigma_e = 230 \text{ MPa}$, and this agrees well with the experiment.

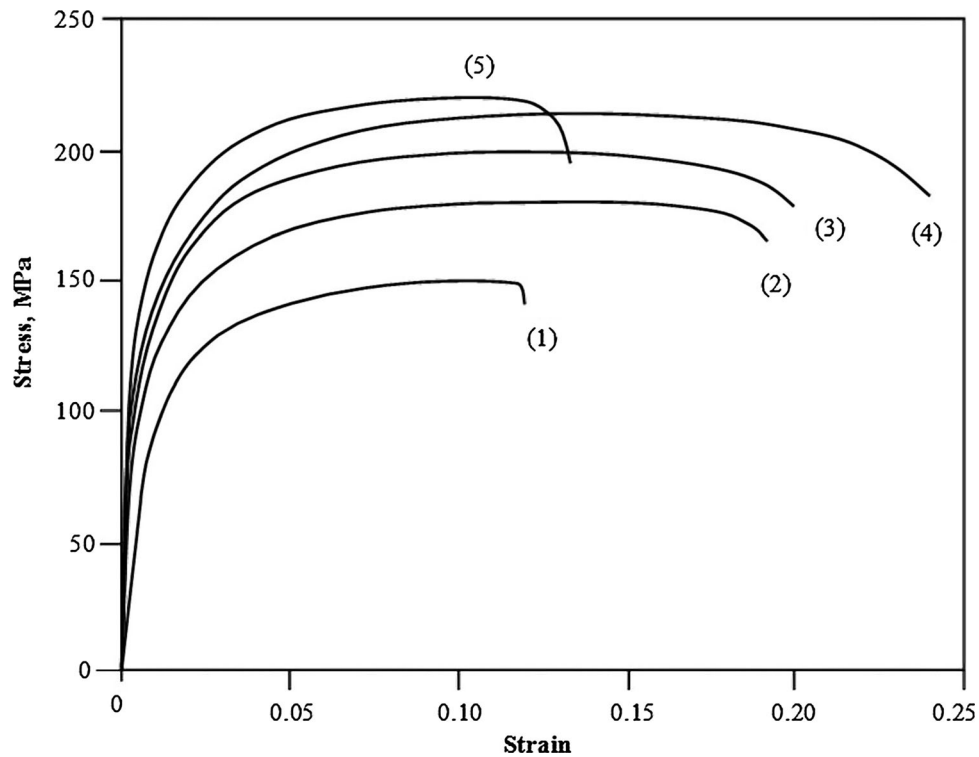


Fig. 19 Stress–strain tension diagrams of samples directionally solidified at the rate of 20 (1), 80 (2), 250 (3), 600 (4), and 1000 (5) $\mu\text{m/s}$. The morphology is predominantly flake (20 and 80 $\mu\text{m/s}$), mixed flake/fiber (250 $\mu\text{m/s}$), fibers (600 and 1000 $\mu\text{m/s}$) (Ref 86)

Therefore, to obtain a hypereutectic alloy of specified composition with a eutectic fiber microstructure, it is necessary to freeze the melt at a rate that ensures the independent coupled solidification of components to form a very fine microstructure (e.g., line 2 in Fig. 1, section 2.1); an alloy of this composition will have the maximum UTS at that freezing rate.

The fracture of hypereutectic alloys is determined by the brittleness of primary silicon crystals. The strength of hypereutectic alloys depends on the shape of primary silicon crystals and the roughness of their surfaces; these determine the stress concentration.

3.2.2 Solidification Rate Effect. In Ref 86, the effect of the solidification rate on the strength of the Al-12 wt.% Si alloy was investigated in the range from 20 to 1000 $\mu\text{m/s}$. The stress–strain tensile diagrams are shown in Fig. 19. A monotonic increase of UTS up to 1000 $\mu\text{m/s}$ is seen. The fracture elongation increased with an increasing solidification rate up to 600 $\mu\text{m/s}$ and then decreased at 1000 $\mu\text{m/s}$. Similar stress–strain behavior and the same UTS and fracture elongation were observed at 1000 $\mu\text{m/s}$ in a study of the effect of Si content (Ref 7).

An analytical model of plastic deformation of Al-Si alloys was developed in Ref 86, based on a mechanical model of dispersion-reinforced metal-matrix composites (Ref 87). According to this model (Ref 86), the stress–strain curves of a composite can be calculated from the stress–strain behavior of its matrix if the elastic modulus and volume fractions of the components are known. It was necessary to take into account the effect of four additional factors on the increase in the effective yield strength of the matrix. One factor is the stress required for dislocations to overcome the barrier of reinforcing particles. The second factor is the effect of the isotropic strain gradient that arises from geometrically necessary dislocations

needed to accommodate the particles. The third factor accounts for the kinematic effects of the strain gradient, taking into account the thermal expansion mismatch between the phases. The effective yield stress and hardening coefficient of the matrix material were taken from experimental tensile behavior for Al-1 wt.% Si (Ref 88); the hardening coefficient was changed slightly to fit the experimental data. The dependence of inter-particle size on the solidification rate of the $V^{-1/2}$ type had been found in Ref 54. Calculated true stress–true strain curves for different solidification rates were in a good agreement with experimental curves. Figure 20 shows the experimental and calculated UTS at strain $\epsilon = 0.1$ for an Al-12 wt.% Si alloy as a function of the average spacing of eutectic microstructures (Ref 86). Both experimental and predicted UTS increased with decreasing spacing, i.e., with increasing solidification rate. The theory had taken into account the only λ and had not considered any morphological transformation. This leads to the conclusion that the increasing UTS is determined mainly by the refinement of the microstructure. The authors (Ref 86) wrote that a good agreement between theoretical and experimental results confirms this conclusion. However, they had assumed that the flake-to-fiber transformation of the eutectic microstructure with increasing V was responsible for the decrease in fracture elongation and some small degree for the increase in flow stress, as observed in Ref 54. The effect of microstructure refinement and the transformation of flake-to-fiber structure were summarized.

Increasing the solidification rate to 600 $\mu\text{m/s}$ caused the UTS and elongation to increase. At this rate, the transformation of the flake-to-fiber microstructure had finished. Increasing the solidification rate to 1000 $\mu\text{m/s}$ caused the UTS to continue to increase but the fracture elongation to decrease. The effect of refinement on an increase in the strength was explained by the

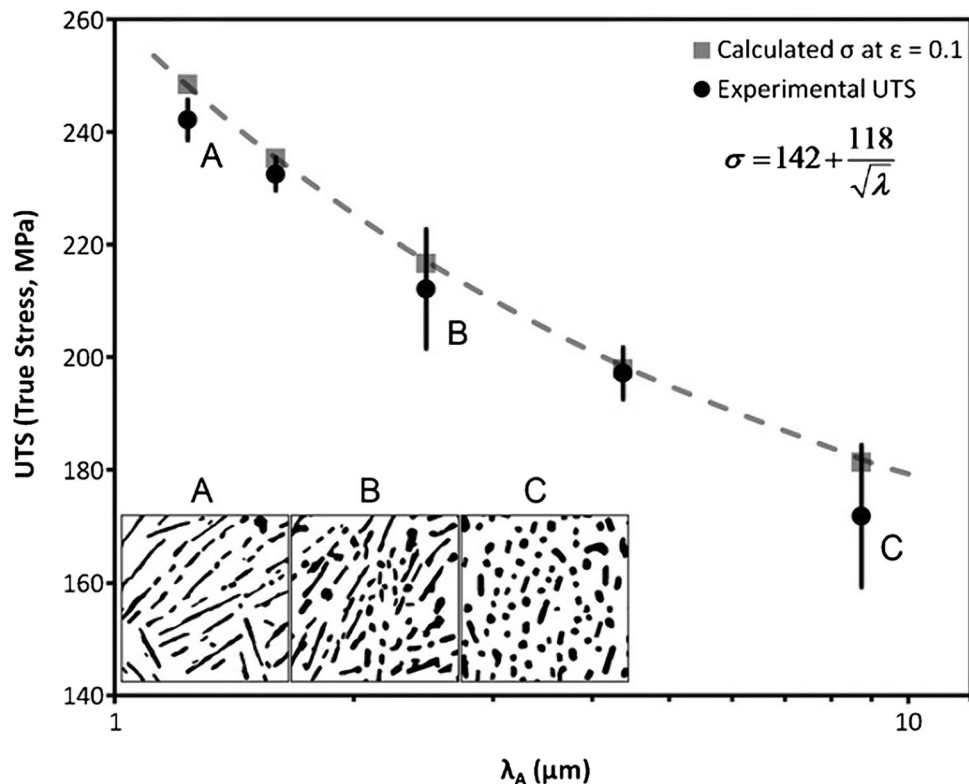


Fig. 20 UTS dependence on the average eutectic spacing. Calculated UTS values were found from calculated flow stresses for a strain equal to 0.1. Average spacing was found according to Ref 54, 86

generation and increase in density of dislocations in the α -Al matrix during cooling due to the mismatch of thermal expansion between eutectic silicon and the α -Al matrix. The increase in elongation of the eutectic alloy during the flake-to-fiber transition was attributed to the transformation of the irregular brittle flake structure to more ductile fiber morphology. Revealing the role of the flake-to-fiber transformation in mechanical properties (Ref 86) provides the opportunity to consciously control the production of an alloy with optimum properties.

The magnitude of the effect of solidification rate on the strength of directionally solidified Al-Si alloys in the range of 10 to 10^3 $\mu\text{m/s}$ can be estimated approximately using the data of Ref 83, 86, 89. By our estimates, the average coefficient of the UTS, $\Delta\sigma_U/\{\sigma_{U0} \times \Delta V\}$, is 0.05 ± 0.015 min/mm. Here, $\Delta\sigma_U$ is the difference in UTS of samples obtained at higher σ and lower σ_0 solidification rates, σ_{U0} is the UTS at lower solidification rate, and ΔV is the difference between these solidification rates. However, the values of UTS reported in Ref 83 were much lower than that in Ref 86, 89. The solidification rate effect on mechanical properties of directionally solidified Al-11.3 wt.% Si samples at a solidification rate higher than 1000 $\mu\text{m/s}$ was studied in Ref 47. The solidification rate dependence of the tensile strength and the elongation in the range from 1.7×10 to 8.3×10^3 $\mu\text{m/s}$ are shown in Fig. 21. In this range of solidification rate, as well as at 103 $\mu\text{m/s}$, the UTS continued to increase, although the effect of the rate on the strength was weaker. The average rate coefficient of UTS $\Delta\sigma_U/\{\sigma_{U0} \times \Delta V\} = 0.014$ min/mm was three tenths of that over the range from 10 to 10^3 $\mu\text{m/s}$. This can be understood if we take into account that the solidification of the alloy with 11.3 wt.% Si was at a higher rate than the 10^3 $\mu\text{m/s}$ yielding a eutectic

microstructure (see Fig. 1). The decrease in the influence of solidification rate on the strength is connected to the shift of the composition required to form a eutectic microstructure. An increase in the volume fraction of primary α -Al dendrites and the refinement of the eutectic microstructure with increasing solidification rate had been observed in Ref 47.

3.2.3 Modification of the Alloys. Modification of Al-Si alloys using chemical, thermal and deformation methods were described in a few reviews (Ref 56, 90-92). Modification of eutectic silicon by different chemical elements was considered in Ref 90. More effective transformation of irregular flake, plate silicon structure to a fine, fibrous and uniform structure takes place when Na or Sr is used. The ratio of their atomic radiuses to that of silicon is about 1.64, which is thought to be the optimal value. There are several theories of chemical modification. Generally, they are based either on a restriction of nucleation of eutectic silicon or on restriction of the growth rate of silicon by a modifier (Ref 93). A more widespread theory connects the modification of a flake-like to a fibrous structure with a change in the intensity of twinning of silicon caused by adsorption of Na (or Sr) on the twin reentrant groove or on growing surfaces of eutectic silicon flake. Na restricts the development of Si flake embryos. This results in a growth of Si fibers.

In review (Ref 91), the primary focus was on modification employing strontium, which is used very widely at present in applications. In that author's opinion the most likely explanation of the chemical modification is removing or neutralizing AlP, which is an effective nucleator for silicon. This results in a fine fibrous eutectic and improves the ductility of the hypoeutectic alloy. Using Sr allows a twofold reduction in the solution heat treatment time, resulting in a cost saving of more than ten

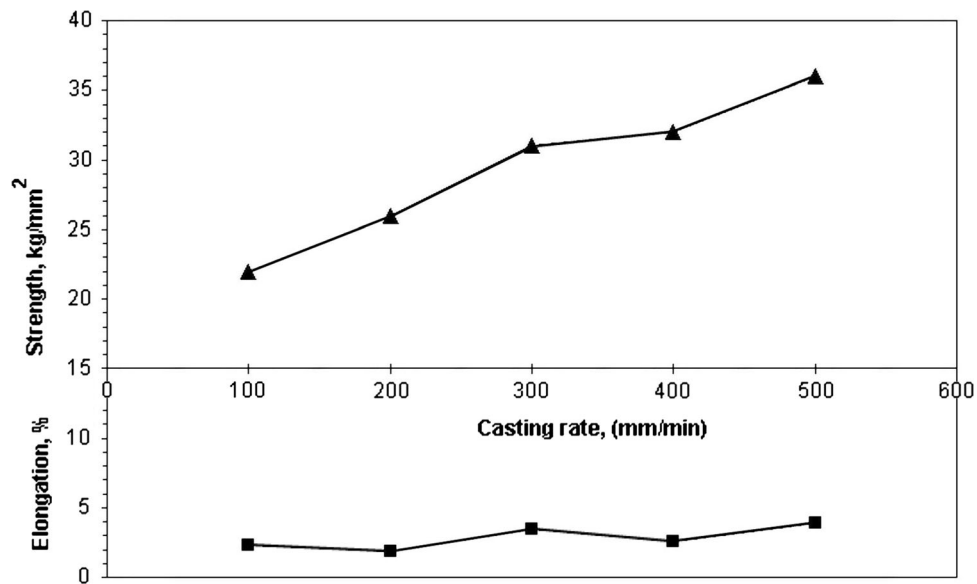


Fig. 21 Influence of casting rate on the strength and elongation of Al-11.3 Si wt.% (Ref 47)

times the cost of the strontium. The author of this very useful review analyzed the effect of modifiers and other chemical elements on the porosity, quality index and American Foundry Society microstructure rating of Al-Si castings. Practical recommendations were given for foundryman on how to obtain a highly modified microstructure. The author noted the necessity to find ways of controlling and limiting the loss of elongation and tensile strength associated with higher iron content, and ways of obtaining super-modified structures with high strength and decreased porosity of castings. There were references to investigations on obtaining super-modified microstructures by stirring during solidification of semi-solid metal (Ref 94) and applying ultrasound to the melt (Ref 95). The author suggests that directional solidification experiments could yield better information on the effect of modifier/refinements and impurities, particularly iron, on the structure and mechanical properties. Discussion on the mechanism of modification of the silicon structure, mainly on the role of oxide biofilms, covering two sides of a silicon wafer, is in Ref 93. The effect of biofilms on Sr modification, porosity and mechanical properties of Al-Si alloys were also considered in review (Ref 96).

The influence of modification on wear resistance and stiffness of hypereutectic alloys was considered in the review (Ref 56). High wear resistance and stiffness, as well as high strength and low temperature expansion, are very important for alloys based on Al-Si in connection with high temperature applications in the automobile industry. Small and well-dispersed silicon particles improve the wear resistance. The eutectic microstructure of unrefined alloy contains needle-like silicon, which creates stress concentrators and initiates an increase and a wide distribution of cracks in the matrix. Moreover, in comparison with refined alloys, unrefined alloys have a larger average penetration of abrasive particles into the surface because of the longer free distance between primary silicon particles of larger size. In a refined alloy, the depth of penetration is less due to the smaller size of primary silicon particles and the shorter average distance between them. The influence of Sr addition on wear volume of Al-20 wt.% Si alloy

was investigated in Ref 97. The wear volume decreases with an increase of Sr to 0.04 wt.% and begins to increase above 0.06 wt.%. The increase in wear resistance can be explained by the refinement of primary silicon that suppresses the creation and propagation of cracks.

The influence of Mg content on the wear resistance of hypereutectic 390 alloys was investigated in Ref 98. It was revealed that the wear resistance increases with an increase in Mg content. Such behavior of the alloy was explained by the formation of Mg₂Si compound that is bonded with the matrix stronger than the coarse primary silicon.

The authors of Ref 56 claim, that hypereutectic alloys are now generally treated with phosphorus to refine the primary silicon. The phosphorus treatment shows no effect on the silicon in the eutectic. Some refining elements have been proposed as an alternative to phosphorus. However, these are only the first attempts to achieve a completely modified structure.

We believe that the investigation (Ref 99) is a new attempt to obtain hypereutectic Al-Si alloy with a super-modified structure. An Al-15 wt.% Si alloy in the shape of a ribbon of 1 m length and 15 × 3 mm² cross section was pulled from the melt by Stepanov's technique. The growth rate was 1 mm/s; the temperature gradient in the cooling zone was about 12 K/mm. Earlier (Ref 7) it had been shown that these conditions correspond to the displacement of the composition yielding a eutectic microstructure. This alloy had a completely fine fiber structure without any primary crystals, corresponding to an AFS rating of five (Ref 100). Modifying this alloy by Sr resulted in the formation of a super-modified eutectic structure with AFS rating 6. Both structures are shown in Fig. 22.

The high plasticity of super-refined alloy results in a high value of the quality index Q (Ref 101) taking into account its ultimate tensile strength σ_B and fracture elongation ε :

$$Q = \sigma_B + k \cdot \log \varepsilon. \quad (\text{Eq 9})$$

For Al-Si alloys, k is equal to 150 (Ref 102). Figure 23 shows the strontium-content dependence of the quality index of Al-15 wt.% Si with eutectic structure (Ref 99) and of A356-T6 alloys (Ref 103). This method of obtaining Al-Si based alloys

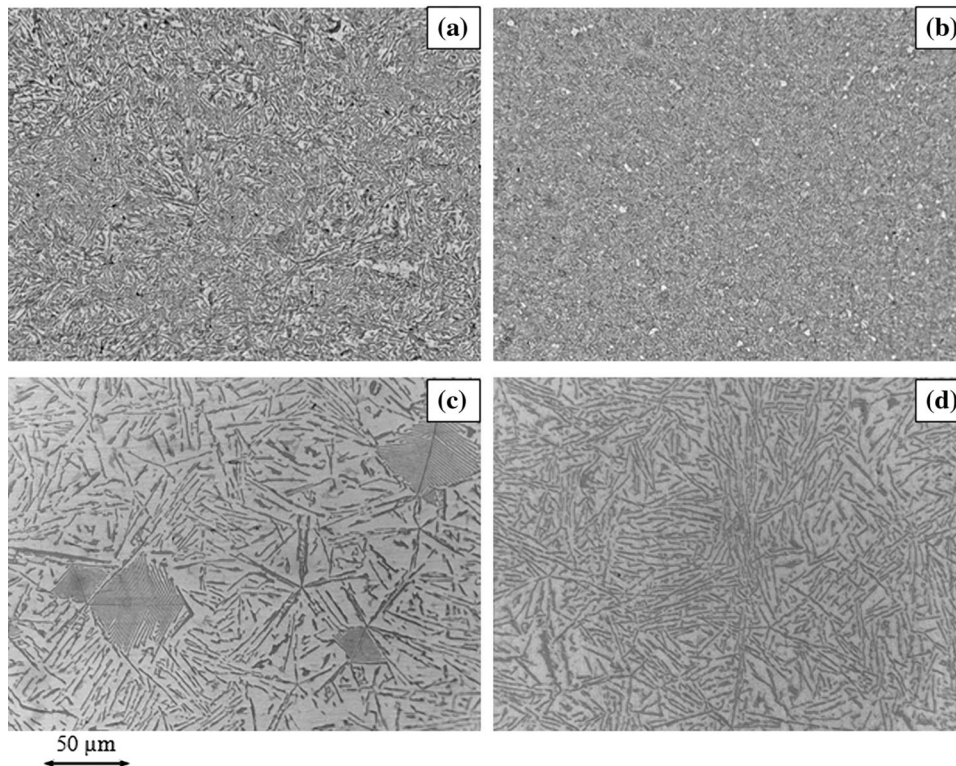


Fig. 22 Microstructure of transverse sections of (a, c)—initial (unmodified) Al-15 Si wt.% alloy and (b, d)—the same alloy modified with 0.01 wt.% Sr. Samples were obtained at solidification rates of (a, b)— $10^3 \mu\text{m/s}$ and (c, d)— $10^2 \mu\text{m/s}$

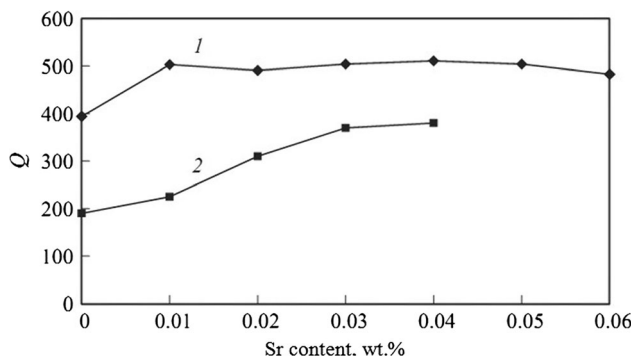


Fig. 23 Quality index as a function of Sr content for: (1) Al-15 Si wt.% alloys, samples with a quasi-eutectic structure (Ref 99), (2) A356-T6 alloy castings with near-eutectic structure (Ref 103)

of hypereutectic composition with a super-modified eutectic structure without any primary crystal seems to have interest for application. However, it is necessary to study the porosity, wear resistance and thermal stability of binary alloys and industrial alloys with different alloying elements obtained by solidification of a melt of hypereutectic composition at a rate that ensures the formation of a fine fiber eutectic structure. It is possible that an alloy of hypereutectic composition with a small 0.01 wt.% Sr having a super-modified eutectic structure would have a small porosity and high wear hardness.

The ultimate tensile strength of this hypereutectic alloy with eutectic structure was 172 MPa. After 0.01 wt. % Sr modification was 277 MPa (Ref 99). By comparison, a modified Al-50 wt.% Si-0.5 wt.% P alloy cast in a permanent mold after heat treatment of T6 had UTS of 160 MPa (Ref 104). A

modified Al-11.3 wt.% Si-0.02 wt.% Sr alloy produced by directional solidification at a speed 1.7 mm/s (about a twofold rate in comparison with Ref 99) had UTS equal to 260 MPa and fracture elongation of 5.5% (Ref 47).

We would like to emphasize also that the observed increased tensile strength and the high elongation for the chosen hypereutectic composition (15 wt.% Si) are obtained at a rate ($10^3 \mu\text{m/s}$) that yields coupled growth of fine fiber eutectic microstructure without any primary crystals. This is maximum value of UTS and was not increased by further increase Si content at a given rate.

In conclusion, we have compared the mechanical properties of alloys obtained by conventional casting and by directional solidification with a controlled rate (Ref 7, 47, 86, 99, 105-108), Table 1. It is seen that maximum UTS and ϵ were obtained in Ref 7) and Ref 99, when solidification occurred at the rate giving coupled growth and resulting in eutectic microstructure for the Si content in the alloy.

The maximum UTS and fracture elongation of Al-Si in Table 1 are close to their minimum values in solidification rate dependences for Ni-Al-based alloys investigated in Ref 11, 12, 109, 110.

4. Nanostructure and Precipitation

Microstructure and its effect on the strength properties of Al-Si alloys obtained by directional solidification were described higher. The microstructure of Al-Si alloys was also investigated at nanoscales. Subgrains of α -Al and precipitates of Si atoms in α -Al have a nanostructure.

Table 1 Mechanical properties of Al-Si alloys obtained by casting in form and directional solidification with controlled rate

<i>N</i>	Material, wt.%	UTS, MPa	Elongation at fracture, %	Chemical modification	Casting method, Solidification rate	References, date
1	Al-13%Si	124	2	...	Sand cast	Ref 105, 1950
		193	13	Na modified	Permanent mold	
		193	3.6	...		
2	A413	221	8	Na modified	Permanent mold	Ref 106, 1977
		198	6,0	...		
		191	12.0	Sr modified		
3	Al-10%Si	141.7	12.2	...	Metal mold	Ref 107, 1999
		154.7	10.3	...		
4	Al-11.3%Si	215	5.5	...	Directional solidification by Ohno method, 1700 $\mu\text{m/s}$	Ref 47, 2000
		250	5.7	0.02%Sr		
5	Al-11.6%Si	215	13.5	0.037%Sr	Gray iron mold	Ref 108, 2001
6	Al-12%Si	222	12.5	...	Bridgman gradient zone directional solidified, 1000 $\mu\text{m/s}$	Ref 86, 2010
7	Al-15%Si	225	13	...	Directional solidification by Stepanov's method, 1000 $\mu\text{m/s}$	Ref 7, 2013
8	Al-15%Si	277	36	0.015%Sr	Directional solidification by Stepanov's method, 1000 $\mu\text{m/s}$	Ref 99, 2016

Table 2 Size of coherent dispersion regions of components of Al-Si alloys

Alloy composition	Component	<i>L</i> , nm	Reference
Al-15 wt.%Si- 0.01 wt.%Sr	α -Al solid solution	93 \pm 20	112
Al-15 wt.%Si	α -Al solid solution	80 \pm 10	V.V. Kaminskii, N.V. Sharenkova, Ioffe Institute, unpublished (2019)
	Eutectic Si	65 \pm 7	

4.1 Microstructural Plasticity and Participation in Binary Al-Si Alloys

Dissipation of energy of mechanical vibrations at small mechanical stresses due to vibration dislocation motion, dislocation internal friction, and a change of Young's modulus due to dislocation displacement at mechanical vibrations, dislocation defect of Young's modulus, in Al-Si alloys were investigated in Ref 7. Al-Si alloys with Si content from 8 to 25 wt.%, solidified at the rate $10^3 \mu\text{m/s}$ were investigated by resonance method at the oscillation frequency about 100 kHz and amplitude ranging from 5×10^{-7} to 3000×10^{-7} . These measurements allowed us to determine the dependence of microplastic flow stress σ_y on Si content of Al-Si alloys for an inelastic strain ε of 5×10^{-8} . We found that $\sigma_y(\varepsilon)$ was a minimum at Al-15 wt.% Si. On the other hand, the yield point was a maximum for Al-15 wt.% Si, which has a eutectic structure (see Fig. 18). This difference seems to be due to the participation of Si atoms in the α -Al solid solution and formation of Guinier–Preston (GP) zones with natural aging at room temperature for alloys obtained at a solidification rate of about $10^3 \mu\text{m/s}$.

Kinetics of silicon precipitation in directionally crystallized binary Al-Si alloys was investigated in Ref 111 by DSC method. The dependencies of the enthalpy of formation of silicon precipitates on temperature and heating rate for samples of different Si content were studied. The effective activation energy of the process was estimated to be 75 ± 5 kJ/mol. The

enthalpy of precipitation of silicon atoms leading to the formation of the Guinier-Preston zones decreases when the silicon content increases from 8 to 15 wt.%.

Oscillation microplastic deformation of dislocations takes place mainly in nanograins in the α -Al solid solution. X ray diffraction analysis of the Al-15% wt. Si alloy (Ref 112) showed that its eutectic structure consisted of regions of coherent dispersion with low-angle boundaries, which are considered to be subgrain boundaries. Table 2 shows the size of the region of coherent dispersion *L* of α -Al solid solution and additional data kindly provided by the authors of this paper. A dislocation displacement on an order of $10^{-1} \mu\text{m}$ in subgrains of sizes of that order can be retarded by Guinier–Preston zones. With increasing silicon content to 15% wt., the contribution of precipitates to a retardation of dislocation oscillation motion decreases as had shown with the help of DSC investigation. In the case of macroplastic tensile deformation, the flow stress will increase with increasing Si content due to increasing volume fraction of the stiffer eutectic structure.

Up to now, there have been no other investigations of participation in binary Al-Si alloys obtained by direction solidification at rate about $10^3 \mu\text{m/s}$. Nevertheless, the results could be compared with the data of the DSC studies of binary Al-Si alloys (Ref 113) obtained by the rotating melt method at high cooling rates to 10^6 K/s. Transmission electron micrograph of Al-11.4 at.% Si alloy ribbon quenched after annealing shown Si particles of irregular spherical shape with 40 nm

average radius. In quenching from liquid state, precipitates had the shape of ribbon of about 40 nm thickness.

In spite of high vacancy density and porosity those alloys, in both cases exotherms of the same alloys measured at the same heating rates are in the near temperature ranges. However, the exothermic peak extreme in Ref 113 was at lower temperature than in Ref 111. The difference about 100 K is due to significantly higher supersaturation and increased instability of α -Al solid solution during solidification at a higher rate. The activation energy of precipitation for alloys obtained by very fast cooling or quenching was ~ 89 kJ/mol in the supersaturated solid solution. This value is higher than the activation energy for the alloy obtained by directional solidification. The high activation energy is explained by the high amount of excess vacancies (Ref 113).

4.2 Precipitation in Commercial Al-Si Alloys

The present review is limited to consideration of directionally solidified binary alloys. But participation plays the most important role for commercial alloys, which usually undergo heat treatment. Here, we consider precipitation during aging and its effect on the mechanical properties of an aged cast Al-Mg-Si alloy to be an exception.

Alloys of this type are widely used in aerospace and civil industries. An Al-0.89 Mg-0.75Si alloy with trace Fe and Zn elements during aging was investigated by transmission electron microscope (TEM), high resolution transmission electron microscope (HRTEM) and hardness measurements (Ref 114). The as-cast ingot was solution heat-treated at 550 °C for 5 h and quenched in ice water. DSC revealed two exothermic peaks at about 250 and 470 °C which are related to the precipitation of metastable β'' and β' phases. TEM and HRTEM revealed the following sequence of precipitations due to the segregation of the solute Mg and Si atoms in Al: Al supersaturated solid solution – GP zone – β'' precipitates – β' precipitates – β precipitates + Si. GP zones were revealed after aging for 5 min at 180 °C. The GP zones had a spherical shape of 5 nm diameter and coherent with Al matrix. β'' precipitates were observed after aging for 1 h at 180 °C. They had a needle shape of about 50 nm length and 4 nm thick. These precipitates with high concentration were semi-coherent with the matrix and inhibited dislocation motion. When the aging time was increased to 5 h and then 10 h, the needle length increased to 150 nm. A small number of large rod-shaped precipitates arose. They were also semi-coherent with the matrix. At the same time, HRTEM reveals β' precipitates of 30-100 nm length and 10-20 nm thickness. After aging at 180 °C for 30 h, metastable β' precipitates of Mg and Si atoms destroyed the coherent relationship with the matrix and transformed into the stable β phase with rectangular plate-shaped morphology. According to EDS analysis, the equilibrium Si phase also arose. Investigations showed strong influence precipitation on the hardness of the alloy. The main strengthening phase is β'' . Maximum hardness after aging was six times the original hardness.

The precipitation sequence observed in Ref 115-118 for Al-Mg-Si alloys was similar to those in Ref 114. In those works, together with β' some other precipitates were observed. Their presence can be explained by different Si and Mg contents as well as different temperatures and times of annealing. In all

observations, peak hardness was reached at high concentration of the metastable, needle-shape β'' phase. This phase is coherent with the Al matrix in the needle direction. But in the plane orthogonal to the needle direction, elastic strains were observed due to lattice mismatch of the needle and α -Al. These stress fields hindered dislocation motion and hardened the alloy. HRTEM and quantitative electron diffraction enabled definition of the monoclinic crystal structure of β'' phase and the orientation relationships to the fcc-matrix of Al (Ref 119):

$$[100]_{\beta''} \parallel [230]_{\text{Al}}, [010]_{\beta''} \parallel [001]_{\text{Al}}, [001]_{\beta''} \parallel [310]_{\text{Al}},$$

with a monoclinic angle of 105.3°.

The experimental determination of the chemical composition of β'' phase was difficult. A study of β'' precipitates by use of high-angle annular dark-field scanning transmission electron microscopy showed $\text{Mg}_4\text{Al}_3\text{Si}_4$ to be the most likely composition (unpublished research, see [10] in Ref 119). Therefore, calculations based on density functional theory using an atomistic model were performed for β'' phase in Ref 119. The enthalpies of formation of several chemical compositions were calculated. The most stable composition was found to be $\text{Mg}_5\text{Al}_2\text{Si}_4$. However, the calculation did not take into account kinetic effects during participate growth.

5. Summary

Aluminum alloys with Al-Si eutectic microstructure are used widely in different fields of modern industry due to their high strength-to-weight ratio, high castability and machinability. There is an increasing demand for improved microstructure and mechanical properties of these alloys.

Controlled fundamental research of the formation of microstructure and the resulting properties of these alloys are being realized with directional solidification experiments. The character of the transformation of flake-to-fine fiber eutectic microstructure with solidification rate has been investigated at a microscopic level. The effects of the solidification rate and cooling rate on the parameters of dendrite structure of the α -Al phase and the average inter-particle space in eutectic microstructures have been studied experimentally and theoretically. The dependence of tensile strength and yield stress on solidification rate and, therefore, on structural parameters has also been revealed. Intensive research has been conducted on the influence of chemical modifiers and thermal modification on the microstructure of Al-Si castings. These works helped to improve technology. However, up to now ways of improvement of conventional technology are explored to obtain commercial Al-Si alloys with a super-modified microstructure without porosity, especially hypereutectic alloys.

We believe that the best cheap solution of this task is solidification of the alloy selected composition at certain cooling rate corresponding to the shifted eutectic point. In that conditions coupled growth of fiber eutectic microstructure takes place. It enables to produce hypereutectic alloys with super-modified structure and much higher ultimate tensile strengths and elongations than conventional casting without controlling cooling. This approach should be taken into account with traditional casting methods at select of the rate of solidification.

Acknowledgments

The authors are very appreciative for the valuable comments and suggestions provided by Prof. W.R. Wilcox, Clarkson University, Potsdam, NY.

References

1. L. Lasa and J.M. Rodriguez-Ibabe, Wear Behavior of Eutectic and Hypereutectic Al-Si-Cu-Mg Casting Alloys Tested Against a Composite Brake Pad, *Mater. Sci. Eng., A*, 2003, **363**, p 193–202
2. Z. Qian, X. Liu, D. Zhao, and G. Zhang, Effects of Trace Mn Additional on the Elevated Temperature Tensile Strength and Microstructure of a Low-Iron Al-Si Piston Alloy, *Mater. Lett.*, 2008, **62**, p 2146–2149
3. J.L. Murray and A.J. McAlister, The Al-Si (Aluminum-Silicon) System, *Bull. Alloy Phase Diagr.*, 1984, **5**(1), p 74–84
4. A.J. McAllister and J.L. Murray, The Al-Ge (Aluminum-Germanium) System, *Bull. Alloy Phase Diagr.*, 1984, **5**(4), p 341–347
5. D.C. Jenkinson and L.M. Hogan, The Modification of Aluminum-Silicon Alloys with Strontium, *J. Cryst. Growth*, 1975, **28**, p 171–187
6. S.P. Nikanorov, M.P. Volkov, V.N. Gurin, Y. Burenkov, L.I. Derkachenko, B.K. Kardashev, L.I. Regel, and W.R. Wilcox, Structural and Mechanical Properties of Al-Si Alloys Obtained by Fast Cooling of a Levitated Melt, *Mater. Sci. Eng., A*, 2005, **390**, p 63–69
7. S.P. Nikanorov, L.I. Derkachenko, B.K. Kardashev, B.N. Korshunov, V.N. Osipov, V.V. Shepizman, Structural and Physicomechanical Properties of Directionally Crystallized Aluminum-Silicon Alloys. *Phys. Solid State*, 2013, **55**(6), p.1207–1213, transl. of original Russian text *Fizika Tverdogo Tela* 2013, **55**(6), p.1119–1125
8. S.P. Nikanorov and V.V. Peller, Shaping by pulling from the melt, *Handbook of Aluminum, Physical Metallurgy and Processes*, G.E. Totten and D.S. MacKenzie, Ed., Marcel Dekker, New York, 2003, p 695–737
9. H.A.H. Steen and A. Hellawel, Structure and Properties of Aluminum-Silicon Eutectic Alloys, *Acta Metall.*, 1972, **20**(3), p 363–370
10. F. Yilmaz and R. Elliot, The Microstructure and Mechanical Properties of Unidirectionally Solidified Al-Si Alloys, *J. Mater. Sci.*, 1989, **24**(6), p 2065–2070
11. L. Wang, J. Shen, Y.-P. Zhang, and L.-L. Guo, Effect of Withdrawal Rate and Gd on the Microstructures and Directionally Solidified NiAl-Cr(Mo) Hypereutectic Alloy, *J. Miner. Metals Mater. Soc. (JOM)*, 2016, **68**, p 1017–1045
12. L. Wang, J. Shen, J. Zhang, and F. Hengzhi, Microstructure, Fracture Toughness and Compressive Property of As-Cast and Directionally Solidified NiAl-Based Eutectic Composite, *Mater. Sci. Eng., A*, 2016, **664**, p 188–194
13. O.L. Rocha, L.G. Gomes, D.J. Moutinho, I.L. Ferreira, and A. Garcia, The Columnar to Equiaxed Transition in the Directional Solidification of Aluminum Based Multicomponent Alloys, *Rem: Revisia Escola de Minas*, 2016, **68**(1), p 85–90
14. M.D. Peres, C.A. Siqueira, and A. Garcia, Macrostructural and Microstructural Development in Al-Si Alloys Directionally Solidified Under Unsteady-State Conditions, *J. Alloy. Compd.*, 2004, **381**(1–2), p 168–181
15. C.A. Siqueira, M. Cheung, and A. Garcia, Solidification Thermal Parameters Affecting the Columnar-to-Equiaxed Transition, *Metall. Mater. Trans. A*, 2002, **33**, p 2107–2118
16. O.L. Rocha, C.A. Siqueira, and A. Garcia, Cellular/Dendritic Transition During Unsteady-State Unidirectional Solidification of Sn-Pb Alloys, *Mater. Sci. Eng., A*, 2003, **347**, p 56–59
17. K.S. Cruz, E.S. Meza, F.A.P. Fernandes, J.M.V. Quaresma, L.C. Casteletti, and A. Garcia, Dendritic Arm Spacing Affecting Mechanical Properties and Wear Behavior of Al-Sn and Al-Si Alloys Directionally Solidified Under Unsteady-State Condition, *Metall. Mater. Trans. A*, 2010, **41**, p 972–984
18. C. Gandin, From Constrained to Unconstrained Growth During Directional Solidification, *Acta Mater.*, 2000, **48**(10), p 2483–2501
19. C.A. Siqueira, M. Cheung, and A. Garcia, The Columnar to Equiaxed Transition During Solidification Sn-Pb Alloys, *J. Alloy. Compd.*, 2003, **351**, p 126–134
20. D.B. Carvalho, E.C. Guimardes, A.L. Moreira, D.J. Moutinho, J.M.D. Filho, and O.L. Rocha, Characterization of the Al-3 wt.% Si Alloy in Unsteady-State Horizontal Directional Solidification, *Materials Research*, 2013, **16**(4), p 874–883
21. J.E. Spinelly, L.L. Ferreira, and A. Garcia, Influence of Melt Convection on the Columnar to Equiaxed Transition and Microstructure of Downward Unsteady-State Directionally Solidified Sn-Pb Alloys, *J. Alloy. Compd.*, 2004, **384**(1), p 217–226
22. R. Triverdi and W. Kurz, Dendritic Growth, *Int. Mater. Rev.*, 1994, **39**(2), p 49–74
23. D.P. Woodruff, *The Solid-Liquid Interface*, Cambridge University Press, London, 1973, p 80–84
24. J.A.E. Bell and W.C. Winegard, Dendrite Spacing in Tin-Lead Alloys, *J. Inst. Met.*, 1963, **93**, p 357–359
25. S.H. Han and R. Trivedi, Primary Spacing Selection in Directionally Solidified Alloys, *Acta Metall.*, 1994, **42**, p 25–41
26. W.W. Mullins and R.F. Sekerka, Morphological Stability of a Particle Growing by Diffusion or Heat Flow, *J. Appl. Phys.*, 1963, **34**, p 323–329
27. G.I. Ding, W. Huang, X. Lin, and Y. Zhou, Prediction of Average Spacing for Constrained Cellular/Dendritic Growth, *J. Cryst. Growth*, 1997, **177**, p 281–288
28. J.A. Warren and J.S. Langer, Prediction of Dendritic Spacing in a Directional Solidification Experiment, *Phys. Rev. E*, 1993, **47**, p 2702–2712
29. L. Makkonen, Spacing in Solidification of Dendritic Arrays, *J. Cryst. Growth*, 2000, **208**, p 772–778
30. E. Gadirh, I. Karaca, H. Kaya, and N. Marash, Effect of Growth Rate and Composition on the Primary Spacing, the Dendrite Tip Radius and Mushy Zone Depth in Directionally Solidified Succinonitrile-Salol Alloys, *J. Cryst. Growth*, 2003, **255**, p 190–203
31. E. Gadirh, N. Marash, B. Bayender, and M. Gunduz, Investigation of the Structure Parameters According to the Solidification Parameters for Pivalic Acid, *J. Mater. Sci.*, 1999, **349**(22), p 5533–5541
32. M. Gunduz and E. Gadirh, Directional Solidification of Aluminum-Copper Alloys, *Mat. Sci. Eng. A*, 2002, **327**(2), p 167–185
33. J.D. Hunt and S.Z. Lu, Numerical Modeling of Cellular/Dendritic Array Growth and Structure Predictions, *Metall. Mater. Trans. A*, 1996, **27A**(3), p 611–623
34. J.S. Langer and H. Muller-Krumbhaar, Theory of Dendritic Growth. I. Elements of a Stability Analyses, *Acta Metall.*, 1978, **26**, p 1681–1687
35. J.D. Hunt, Cellular and Primary Dendrite Arm Spacings, *Solidification and Casting of Metals*, J.D. Hunt, Ed., The Metal Society, London, 1979, p 3–9
36. W. Kurz and D.J. Fisher, Dendrite Growth at the Limit of Stability: Tip Radius and Spacing, *Acta Metall.*, 1981, **29**(1), p 11–20
37. R. Trivedi, Interdendritic Spacing: Part II. A Comparison of Theory and Experiment, *Metall. Trans.*, 1984, **15A**, p 977–982
38. D. Bouchard and J.S. Kirkaldy, Prediction of Dendrite Arm Spacing in Unsteady and Steady-State Heat Flow of Unidirectionally Solidified Binary Alloys, *Metall. Mater. Trans.*, 1997, **28B**, p 651–663
39. K. Trivedi and K. Somboonsuk, Constrained Dendritic Growth and Spacing, *Mater. Sci. Eng.*, 1984, **65**, p 65–74
40. J.W. Rutter and B. Chalmers, A prismatic Substructure Formed During Solidification of Metals, *Can. J. Phys.*, 1953, **31**, p 15–39
41. W.A. Tiller, K.A. Jackson, J.W. Rutter, and B. Chalmers, The Redistribution of solute Atoms During the Solidification of Metals, *Acta Metall.*, 1953, **1**, p 428–437
42. H. Kaya, E. Gadirh, and M. Gunduz, Dendritic Growth in an Aluminum-Silicon Alloy, *J. Mater. Eng. Perform.*, 2007, **6**(1), p 12–21
43. J.E. Spinelly, D.M. Rosa, I.L. Ferreira, and A. Garcia, Influence of Melt Convection on Dendritic Spacings of Downward, Unsteady-State Directionally Solidified Al-Cu Alloys, *Mater. Sci. Eng.*, 2004, **383A**, p 271–282
44. J.E. Spinelly, M.D. Peres, and A. Garcia, Thermosolutal Convective Effects on Dendritic Array Spacings in Downward Transient Directional Solidification of Al-Si Alloys, *J. Alloy. Compd.*, 2005, **403**, p 228–238
45. O.L. Rocha, C.A. Siqueira, and A. Garcia, Heat Flow Parameters Affecting Dendrite Spacing During Unsteady-State Solidification of Sn-Pd and Al-Cu Alloys, *Metall. Mater. Trans. A*, 2003, **34A**, p 995–1006

46. D.L.B. Carvalho, T.A.P.S. Costo, A.L.S. Moreiro, M.A.P.S. Silva, J.M.D. Filho, D.J.C. Moutinho, and O.F.L. Rocha, Solidification Thermal Parameters and Dendritic Growth During the Horizontal Directional Solidification of Al-7 wt.% Si alloy, *REM: Rev Min*, 2014, **67**(3), p 267–270
47. M.H. Kim, C.H. Jung, H.H. Jo, and C.S. Kang, The Effect of Ti and Sr on the Microstructures of Al-11.3 wt.% Si Alloys Produced by the Ohno Continuous Casting Process, *Metals Mater.*, 2000, **6**(3), p 235–240
48. H. Soda, F. Chabchoub, W.H. Lam, S.A. Argyropoulos, and A. Mclean, The horizontal Ohno Continuous Casting Process, *Cast Metals*, 1991, **4**, p 12–19
49. A. Ohno, Continuous Casting of Single Crystal ingots by O.C.C. process, *J. Metals*, 1986, **38**, p 14–16
50. B. Toloui and A. Hellawell, The Separation and Undercooling in Al-Si Eutectic Alloy—The Influence of Freezing Rate and Temperature Gradient, *Acta Metall.*, 1976, **24**(6), p 565–573
51. P. Magnin, J.T. Mason, and R. Trivedi, Growth of Irregular Eutectics and the Al-Si System, *Acta Metall. Mater.*, 1991, **39**(4), p 469–480
52. S. Khan and R. Elliot, Quench Modification of Aluminum-Silicon Eutectic Alloys, *J. Mater. Sci.*, 1996, **31**(14), p 3731–3737
53. R. Cupris, B. Major, and W. Wolczynsky, Transition of Flake into Fibre Structure in Eutectic Al-Si, *Mater. Sci. Forum*, 2000, **329–330**, p 161–166
54. T. Hosch, L.G. England, and R.E. Napolitano, Analysis of the High Growth-Rate Transition in Al-Si Eutectic Solidification, *J. Mater. Sci.*, 2009, **44**(18), p 4892–4899
55. H.S. Kang, W.Y. Yoon, K.H. Kim, M.H. Kim, and Y.P. Yoon, Microstructure Selections in the Undercooled Hypereutectic Al-Si Alloys, *Mater. Sci. Eng., A*, 2005, **404**(1–2), p 117–123
56. V.K. Vijeesh and N. Prabhu, Review of Microstructure Evolution in Hypereutectic Al-Si Alloys and Its Effect on Wear Properties, *Trans. Indian Inst. Met.*, 2014, **67**(1), p 1–18
57. H. Yi and D. Zhang, Morphologies of Si Phase and La-rich Phase in As-Cast Hypereutectic Al-Si-xLa Alloys, *Mater. Lett.*, 2003, **57**, p 2523–2529
58. Y.T. Pey and J. De Hosson, Functionally Graded Materials Produced by Laser Cladding, *Acta Mater.*, 2000, **48**, p 2617–2624
59. Y.T. Pey and J. De Hosson, Five-Fold Branched Si Particles in Laser Clad AlSi Functionally Graded Materials, *Acta Mater.*, 2001, **49**, p 561–571
60. D. Liang, D. Bayraktar, and H. Jones, Formation and Segregation of Primary Silicon in Bridgman Solidification Al-18.3 wt.% Si Alloy, *Acta Metall. Mater.*, 1995, **43**, p 579–585
61. W.M. Wang, X.F. Bian, J.Y. Oin, and S.I. Syliusarenko, The Atomic-Structure Changes in Al-16% Si Alloy Above the Liquidus, *Metall. Mater. Trans. A*, 2000, **31**, p 2163–2166
62. C.L. Xu, H.Y. Wang, F. Qiu, Y.F. Yang, and Q.C. Jiang, Cooling Rate and Microstructure of Rapidly Solidified Al-20 wt.% Si Alloy, *Mater. Sci. Eng., A*, 2006, **417**, p 275–280
63. P.J. Li, V.I. Nikitin, E.G. Kandalova, and K.V. Nikitin, Effect of Melt Overheating, Cooling and Solidification Rates on Al-16 wt.% Si Alloy Structure, *Mater. Sci. Eng., A*, 2002, **332**, p 371–374
64. X.F. Bian and W.M. Wang, Thermal-Rate Treatment and Structure Transformation of Al-13 wt.% Si Alloy, *Metall. Mater. Lett.*, 2000, **44**, p 54–58
65. C.L. Xu and Q.C. Jiang, Morphologies of Primary Silicon in Hypereutectic Al-Si Alloys with Melt Overheating Temperature and Cooling Rate, *Mater. Sci. Eng., A*, 2006, **437**, p 451–455
66. C.L. Xu, H.Y. Wang, C. Liu, and Q.C. Jiang, Growth of Octahedral Primary Silicon in Cast Hypereutectic Al-Si alloys, *J. Cryst. Growth*, 2006, **291**, p 540–547
67. F. Yilmaz, O.A. Atasoy, and R. Elliot, Growth Structures in Aluminium-Silicon Alloys II. The Influence of Strontium, *J. Cryst. Growth*, 1992, **118**, p 377–384
68. R.P. Liu, D.M. Herlach, M. Vandyousseffi, and A.L. Greer, Undercooling and Solidification of Al-50 at. pct. Si Alloy by Electromagnetic Levitation, *Metall. Mater. Trans. A*, 2004, **35**(2), p 607–612
69. M.G. Day, Primary Silicon Spherulites in Aluminum-Silicon Alloys, *Nature*, 1968, **219**, p 1357–1358
70. K.F. Kobayashi and L.M. Hogan, The Crystal Growth of Silicon in Al-Si Alloys, *J. Mater. Sci.*, 1985, **20**, p 1961–1975
71. H. Fredriksson, M. Hillert, and N. Lange, The Modification of Aluminium-Silicon Alloys by Sodium, *J. Inst. Metals*, 1973, **101**, p 285–299
72. C.B. Kim, R.W. Heine, Fundamentals of Solidification in the Aluminum Silicon System. *J. Inst. Metals*, 1963-64, **92**, 367–376
73. A. Hellawell, The Growth and Structure Eutectics with Silicon and Germanium, *Prog. Mater. Sci.*, 1970, **15**, p 3–78
74. K. Kobayashi, P.H. Shingu, and R. Ozaki, Crystal Growth of the Primary Silicon in an Al-16 wt.% Si Alloy, *J. Mater. Sci.*, 1975, **10**, p 290–299
75. L.I. Derkachenko, B.N. Korchunov, S.P. Nikanorov, V.N. Osipov, and V.V. Shpeizman, Structure, Microhardness and Strength of a Directionally Crystallized Al-Ge Alloy. *Phys. Solid State*, 2014, **56**(3), pp. 527-530, (transl. of original Russ. text Fizika Tverdogo Tela, 2014, **56**(3), p.512-513)
76. V.M. Glazov and V.N. Vigdorovich, *Microhardness of metals, State science technical publishing house on ferrous and non-ferrous metallurgy*, Moscow, 1962, (Gos. Nauch. Tekhn. Izd. Literaturny po Chernoi i Tsvetnoi Metallurgii, in Russian)
77. S. Justl and R.H. Bragg, Vickers Hardness Measurements of Unidirectionally Solidified Al-Si Eutectic Alloy Grown at Different Rates, *Met. Trans. AIME*, 1976, **7A**, p 1954–1957
78. S. Justl and R.H. Bragg, Tensile Properties of Directionally Solidified Al-Si Eutectic, *Metall. Trans. AIME*, 1978, **9A**, p 515–518
79. H. Kaya, E. Cadirli, M. Gunduz, and A. Ulgen, Effect of the Temperature Gradient, Growth Rate, and the Interflake Spacing on the Microhardness in the Directionally Solidified Al-Si Eutectic Alloy, *J. Mater. Eng. Perf.*, 2003, **12**(5), p 544–551
80. S. Khan, A. Ourdjini, Q.S. Hamed, M.A.A. Najafabadi, and R. Elliott, Hardness and Mechanical Property Relationship in of Directionally Solidified Aluminum-Silicon Eutectic alloys with Different Silicon Morphologies, *J. Mater. Sci.*, 1993, **28**, p 5957–5962
81. A.I. Telli and S.E. Kisakurek, Effect of Antimony Additions on Hardness and Tensile Properties of Directionally Solidified Al-Si Eutectic Alloy, *Mater. Sci. Technol.*, 1988, **4**, p 153–156
82. F. Yilmaz, Structure and Properties of Directionally Solidified Al-Si Hypereutectic Alloys, *Mater. Sci. Eng., A*, 1990, **124A**, p L1–L5
83. F. Vnuk, M. Sahoo, R. Van De Merve, and R.W. Smith, The Hardness of Al-Si Eutectic Alloys, *J. Mater. Sci.*, 1979, **14**, p 975–987
84. G.B. Stroganov, V.A. Rotenberg, G.B. Gershman, (Splav Aluminiya s Kremniem (Alloys of aluminum with silicon), Metallurgy, Moscow, 1977, p.121 (in Russian))
85. E.H. Dix, Jr. and J.J. Bowman, *Metals Handbook*, T. Lyman, Ed., American Society for Metals, Metals Handbook Committee, Cleveland, OH, 1948, p. 804
86. T. Hosch and R.E. Napolitano, The Effect of the Flake to Fiber Transition in Silicon Morphology on the Tensile Properties of Al-Si Eutectic Alloys, *Mater. Sci. Eng., A*, 2010, **528**(1), p 226–232
87. C.W. Nan and D.R. Clarke, The Influence of Particle Size and Particle Fracture on the Elastic/Plastic Deformation of Metal Matrix Composites, *Acta Mater.*, 1996, **44**(9), p 3801–3811
88. M.T. Kiser, F.W. Zok, and D.S. Wilkinson, Plastic Flow and Fracture Metal of a Particulate Metal Matrix Composite, *Acta Materialia*, 1996, **44**(9), p 3465–3476
89. V.Yu. Fedorov, S.B. Kustov, and R. Shaller, Growth Parameters Dependence of Microstructure Dispersion of Aluminum Alloys, *Bull. Russ. Acad. Sci. Phys.*, 2004, **68**, p 865–869 (in Russian)
90. S. Hegde and K.N. Prabhu, Modification of Eutectic Silicon in Al-Si alloys, *J. Mater. Sci.*, 2008, **43**, p 3009–3027
91. G.K. Sigworth, The Modification of Al-Si Casting Alloys: Important Practical and Theoretical Aspects, *Int. J. Metalcast.*, 2008, **2**(2), p 19–41
92. G.K. Sigworth, The modification of Al-Si casting alloys: Important practical and theoretical aspects (Author's Reply). *Int. J. Metalcast.* 2009, **3**(1), p. 65–67, 68–70, 71–72
93. L. Qiang, L. Qingchun, and L. Qiful, Modification of Al-Si Alloys with Sodium, *Acta Metall. Mater.*, 1991, **39**(11), p 2497–2502
94. S. Nafisi and R. Ghomashchi, Effect of Modification During Conventional and Semi-Solid Metal Processing of A356 Al-Si Alloy, *Mater. Sci. Eng., A*, 2006, **415**, p 273–285
95. X. Jian, C. Xu, T. Meek, and Q. Han, Effect of Ultrasound Vibration on the Solidification Structure of A356 Alloy, *AFS Trans.*, 2005, **113**, p 131–138

96. J. Campbell and M. Tiryakioglu, Review of Effect of P and Sr on Modification and Porosity Development in Al-Si Alloys, *Mater. Sci. Technol.*, 2010, **26**(3), p 262–268
97. G. Liu, G. Li, C. Anhui, and Z. Chen, The Influence of Strontium Addition on Wear Properties of Al-20 wt.% Si Alloys Under Dry Reciprocating Sliding Condition, *Mater. Des.*, 2011, **32**(1), p 121–126
98. A. Hekmat-Ardakan, X. Liu, F. Ajersh, and X.G. Chen, Wear Behavior of Hypereutectic Al-Si-Cu-Mg Casting Alloys with Variable Mg Contents, *Wear*, 2010, **269**, p 684–692
99. A.I. Averkin, B.N. Korchunov, S.P. Nikanorov, V.N. Osipov, The effect of strontium on the mechanical properties of aluminum-silicon alloy, *Tech. Phys. Lett.*, 2016, **42**(2), p.201–203, (transl. of original Russian text, *Pis'ma v ZhTF*, 2016, **42**, p.67–73)
100. G.K. Sigworth, Determining Grain Size and Eutectic Modification in Aluminum Alloy Castings, *Modern Casting*, 1987, **77**, p 23–25
101. M. Drouzy, S. Jakob, and M. Richard, Interpretation of Tensile Results by Means of Quality Index and Probable Yield Strength, *AFS Int. Cast. Metals J.*, 1980, **5**, p 43–50
102. A.M. Samuel, J. Gauthier, and F.H. Samuel, Microstructural Aspects of the Dissolution and Melting of Al₂Cu Phase in Al-Si Alloys During Solution Heat Treatment, *Metall. Mater. Trans. A*, 1996, **27**, p 1785–1798
103. B. Closset and J.E. Gruzleski, Mechanical Properties of A356 Alloy Modified with Pure Strontium, *Am. Found. Soc. (AFS) Trans*, 1982, **90**, p 453–464
104. F. Cao, Y. Jia, K.G. Prashanth, P. Ma, J. Liu, S. Scudino, F. Huang, J. Eckert, and J. Sun, Evolution of Microstructure and Mechanical Properties of As-Cast Al-50Si Alloy Due to Heat Treatment and P Modifier Content, *Mater. Des.*, 2015, **74**, p 150–156
105. B.M. Thall and B. Chalmers, Modification in Aluminum Silica Alloys, *J. Inst. Metals.*, 1950, **77**, p 79–97
106. F. Fommei, Modification Treatments of Al-Si Alloys, *Aluminio*, 1977, **46**, p 121–135
107. M. Gupta and S. Ling, Microstructure and Mechanical Properties of Hypo/Hypereutectic Al-Si Alloys Synthesized Using a Near-Net Shape Forming Technique, *J. Alloy. Compd.*, 1999, **287**, p 284–294
108. H. Liao, Y. Sun, and G. Sun, Correlation Between Mechanical Properties and Amount of Dendritic α -Al Phase in As-Cast Near-Eutectic Al-11.6% Si Alloys Modified with Strontium, *Mater. Sci. Eng., A*, 2002, **335**, p 62–66
109. L. Wang, J. Shen, Z. Shang, J. Zhang, J. Chen, and F. Hengzhi, Effect of Dy on the Microstructures of Directionally Solidified NiAl-Cr(Mo) Hypereutectic Alloy at Different Withdrawal Rates, *Intermetallics*, 2014, **44**, p 44–54
110. L. Wang, J. Shen, Z. Shang, J. Zhang, D. Yujun, and F. Hengzhi, Microstructure and Mechanical Property of Directionally Solidified NiAl-Cr(Mo)-(Hf, Dy) Alloy at Different Withdrawal Rates, *Mater. Sci. Eng., A*, 2014, **607**, p 113–121
111. L.M. Egirova, B.N.Korchunov, V.N. Osipov, V.A. Bershtein, S.P. Nikanorov, Kinetics of Silicon Precipitation in a Directly Crystallized Binary Al-Si Alloy, *Phys. Solid State*, 2013, **55** (12), p.2549–2553, (transl. of original Russian text, *Fisika Tverdogo Tela*, 2013, **55** (12), p.2423–2427)
112. S.P. Nikanorov, B.K. Kardashev, V.N. Osipov, V.V. Kaminscii, and N.V. Sharenkova, Anelasticity and Nanostructural Dislocation Deformation of Al-Si Alloy with Supermodified Eutectic Structure, *J. Tech. Phys.*, 2019, **8**, p 1151–1154
113. M. Van Rooyen and E.J. Mittemeijer, Precipitation of Silicon in Aluminum-Silicon: A Calorimetric Analysis of Liquid-Quenched and Solid-Quenched Alloys, *Metall. Trans. A*, 1989, **20**, p 1207–1214
114. X. Fang, M. Song, K. Li, and Y. Du, Precipitation Sequence of an Aged Al-Mg-Si Alloy, *J. Min. Metall. Sect. (B)*, 2010, **46**(2), p 171–180
115. K. Matsuda, Y. Sakaguchi, Y. Miyata, Y. Uetani, T. Sato, A. Kamia, and S. Ikeno, Precipitation Sequence of Various Kinds of Metastable Phases in Al-1.0 mass% Mg₂Si-0.4 mass% Si alloy, *J. Mater. Sci.*, 2000, **35**, p 179–189
116. C.D. Marioara, S.J. Andersen, H.W. Zandbergen, and R. Holmstad, The Influence of Alloy Composition on Precipitates of the Al-Mg-Si System, *Metall. Mater. Trans. A*, 2005, **36**, p 691–702
117. S.J. Andersen, C.D. Marioara, R. Vissers, A. Frøseth, and H.W. Zandbergen, The Structural Relation Between Precipitates in Al-Mg-Si Alloys, the Al-Matrix and Diamond Silicon, with Emphasis on the Trigonal Phase U1-MgAl₂Si₂, *Mater. Sci. Eng., A*, 2007, **444**, p 157–169
118. S.J. Andersen, H.W. Zandbergen, J. Jansen, C. Trehold, U. Tundal, and O. Reiso, The Crystal Structure of the β'' Phase in Al-Mg-Si Alloys, *Acta Mater.*, 1998, **46**(9), p 3283–3298
119. P.H. Ninive, O.M. Lovvik, and A. Strandlie, Density Functional Study of the β'' Phase in Al-Mg-Si alloys, *Metall. Mater. Trans. A*, 2014, **45**, p 2916–2924

Publisher's Note Springer Nature remains neutral with regard to jurisdictional claims in published maps and institutional affiliations.